JGR Atmospheres

RESEARCH ARTICLE
10.1029/2019JD032356

This article is a companion to Vautard et al. (2021), https://doi.org/10.1029/2019JD032344.

Key Points:

- This paper presents the first of this size regional climate model ensemble to investigate and understand the climate change response over the whole of Europe
- The paper confirms previous findings for mean and extreme climate change but is able to show the added value information of the high-resolution regional ensemble
- The paper assesses the regional and global model consensus in the projection and presents also the uncertainty of the signal

Correspondence to:
E. Coppola,
coppolae@ictp.it

Citation:
Coppola, E., Nogherotto, R., Ciarlo', J. M., Giorgi, F., van Meijgaard, E., Kadygrov, N., et al. (2021). Assessment of the European Climate Projections as Simulated by the Large EURO-CORDEX Regional and Global Climate Model Ensemble. *Journal of Geophysical Research: Atmospheres*, *126*, e2019JD032356. https://doi.org/10.1029/2019JD032356

Received 31 DEC 2019
Accepted 18 SEP 2020
Accepted article online 20 NOV 2020

Assessment of the European Climate Projections as Simulated by the Large EURO-CORDEX Regional and Global Climate Model Ensemble

Erika Coppola[1], Rita Nogherotto[1], James M. Ciarlo'[1], Filippo Giorgi[1], Erik van Meijgaard[2], Nikolay Kadygrov[3], Carley Iles[3], Lola Corre[4], Marit Sandstad[5], Samuel Somot[6], Pierre Nabat[6], Robert Vautard[3], Guillaume Levavasseur[3], Clemens Schwingshackl[5], Jana Sillmann[5], Erik Kjellström[7], Grigory Nikulin[7], Emma Aalbers[2], Geert Lenderink[2], Ole B. Christensen[8], Fredrik Boberg[8], Silje Lund Sørland[9], Marie-Estelle Demory[9], Katharina Bülow[10], Claas Teichmann[10], Kirsten Warrach-Sagi[11], and Volker Wulfmeyer[11]

[1]The Abdus Salam International Center for Theoretical Physic (ICTP), Trieste, Italy, [2]Royal Netherlands Meteorological Institute (KNMI), De Bilt, The Netherlands, [3]Laboratoire des Sciences du Climat et de l'Environnement, Institut Pierre-Simon Laplace (IPSL), Gif sur Yvette, France, [4]Meteo-France, Toulouse, France, [5]Center for International Climate Research (CICERO), Oslo, Norway, [6]CNRM, Université de Toulouse, Météo-France, CNRS, Toulouse, France, Toulouse, France, [7]Swedish Meteorological and Hydrological Institute, Norrköping, Sweden, [8]Danish Meteorological Institute, Copenhagen, Denmark, [9]Institute for Atmospheric and Climate Science, ETH Zurich, Zürich, Switzerland, [10]Climate Service Center Germany (GERICS), Helmholtz-Zentrum Geesthacht, Hamburg, Germany, [11]Institute of Physics and Meteorology, University of Hohenheim, Stuttgart, Germany

Abstract This paper analyzes the ensemble of regional climate model (RCM) projections for Europe completed within the EURO-CORDEX project. Projections are available for the two greenhouse gas concentration scenarios RCP2.6 (22 members) and RCP8.5 (55 members) at 0.11° resolution from 11 RCMs driven by eight global climate models (GCMs). The RCM ensemble results are compared with the driving CMIP5 global models but also with a subset of available last generation CMIP6 projections. Maximum warming is projected by all ensembles in Northern Europe in winter, along with a maximum precipitation increase there; in summer, maximum warming occurs in the Mediterranean and Southern European regions associated with a maximum precipitation decrease. The CMIP6 ensemble shows the largest signals, both for temperature and precipitation, along with the largest inter-model spread. There is a high model consensus across the ensembles on an increase of extreme precipitation and drought frequency in the Mediterranean region. Extreme temperature indices show an increase of heat extremes and a decrease of cold extremes, with CMIP6 showing the highest values and EURO-CORDEX the finest spatial details. This data set of unprecedented size and quality will provide the basis for impact assessment and climate service activities for the European region.

1. Introduction

Despite decades of efforts, the characterization of future climate evolutions at regional to local scales over Europe remains an open challenge which requires (1) a large ensemble to cover all uncertainty sources (Deser et al., 2012; Hawkins & Sutton, 2009) and to explore all potential future conditions; (2) a high-resolution description of regional climate phenomena that can locally modify the climate change signal, for example, due to islands, cities, and coastal or mountain areas (e.g., Giorgi et al., 2016). So far, achieving both aspects in the same modeling exercise has been impossible mostly due to limitations in computer power and international coordination. Typically, successive CMIP (Coupled Model Intercomparison Project) initiatives based on global climate models (GCMs) have been able to provide large ensembles that cover reasonably well the various uncertainty sources but at too coarse spatial and temporal resolution to describe climate at regional to local scales. On the other hand, projects based on high-resolution regional climate models (RCMs), such as PRUDENCE (Christensen & Christensen, 2007), ENSEMBLES (Hewitt & Griggs, 2004; Van der Linden, 2009), Med-CORDEX (Ruti et al., 2016; Somot et al., 2018) or EURO-CORDEX (Jacob et al., 2014), have not been able to reach an ensemble size which would cover sufficiently well the uncertainty range in future climate projections. For example, the PRUDENCE ensemble was mostly based on one driving

GCM, the ENSEMBLES ensemble focused on one scenario and was limited to about 20 simulations (Déqué et al., 2012; Kjellström et al., 2013; Vautard et al., 2014), and early EURO-CORDEX-based studies at 12 km spatial resolution were limited to a small ensemble size per socio-economic scenario, typically ranging from about 10 runs (Jacob et al., 2014; Tramblay & Somot, 2018) to about 20 runs (Kjellström et al., 2018).

Analyses of these previous ensembles showed some consistent signals over the European region. Both winter and summer are projected to become warmer throughout Europe, with the warming being strongest in winter over Northern Europe and in summer over the Mediterranean and northernmost Scandinavia close to the Arctic (Christensen et al., 2019; Giorgi & Lionello, 2008; Jacob et al., 2014; Kjellström et al., 2018). Extreme warm events are projected to increase, along with a higher number of heat waves across Europe (Jacob et al., 2014; Kjellström et al., 2018; Russo et al., 2015) and substantial increasing trends in various heat stress indicators. Conversely, extreme cold events in winter are projected to decrease in frequency and intensity (Vautard et al., 2014).

Some consistent precipitation change signals have also been found. During winter, seasonal precipitation totals are projected to increase in the northern half of Europe, and to show a more uncertain change signal in the south. In summer, projections show a substantial decrease of precipitation over most of central and southern Europe, with a maximum in the Western Mediterranean basin and over Spain and France, while a small increase is projected for the Scandinavian region. In fact, the Mediterranean region was identified as a climate change drought hot spot by Giorgi (2006), Giorgi and Lionello (2008) and Mora et al. (2018), Spinoni et al. (2020), while Ruosteenoja et al. (2018) showed an increased probability of drought in the Mediterranean based on soil moisture and Giorgi et al. (2018) and Spinoni et al. (2014, 2020) reached the same conclusions using precipitation deficit indices. Independent of the scenario and the temporal horizon, the precipitation change zero line crosses continental Europe with a substantial uncertainty concerning its position (Giorgi & Coppola, 2007; Jacob et al., 2014; Kjellström et al., 2018). Extreme precipitation is projected to increase throughout the entire European territory, although with a less certain signal in the southernmost Mediterranean basin (Hodnebrog et al., 2019; Jacob et al., 2014; Rajczak & Schär, 2017; Tramblay & Somot, 2018).

Recently, the EURO-CORDEX projection ensemble has been enhanced as part of the European Copernicus Climate Change Service (C3S), resulting in a high-resolution (0.11°) ensemble of unprecedented size (Jacob et al., 2020). This offers the opportunity, on the one hand, to have a more thorough validation of observed climate statistics (Kotlarski et al., 2014; Vautard et al., 2014, 2020) and past climate trends (Christensen et al., 2019; Nabat et al., 2014) and, on the other hand, to produce a more robust assessment of climate change projections over the European region and in particular a better characterization of uncertainties associated with mean signals. The companion paper by Vautard et al. (2020) presents an assessment of the model ensemble performance in reproducing different characteristics of present-day climate, while here we focus on the climate change signal for temperature and heat-related indices, along with precipitation and wet and dry indices relevant for impacts and climate hazard assessment. An analysis is also presented of solar radiation reaching the surface. The purpose of this paper is to provide a basic reference for users of the EURO-CORDEX ensemble but, although we include a relatively wide range of indicators, we recognize that there are many more which could be investigated in future work based on targeted applications. We present both high-resolution maps of changes in the selected indices and results aggregated over the three European sub-regions defined in Iturbide et al. (2020).

The second aim of the paper is to measure the degree of consistency between the EURO-CORDEX 12-km resolution large ensemble and its driving GCM ensemble, which is a sub-sample of the CMIP5 ensemble. Finally, we also assess the first set of available CMIP6 GCMs in order to illustrate how the higher climate change sensitivity and stronger warming found in the CMIP6 GCMs (Forster et al., 2020) is translated at the European scale. The ensembles and indices considered in this paper are described in section 2, while results are discussed in section 3 and discussion and conclusions presented in section 4.

2. Data and Methods

2.1. Multimodel Ensembles of Climate Projections

The regional climate projection ensemble includes 55 scenario simulations for the RCP8.5 and RCP2.6 scenarios at 0.11° resolution over the common EURO-CORDEX domain using 8 driving GCMs and 11

Table 1
EURO-CORDEX RCMs and Their Corresponding Driving GCM (With Variant Label) Variable Used in This Study

Driving CMIP5 GCM	Variant	RCM	tas	tasmin	tasmax	q	pr	rsds
CCCma-CanESM2	r1i1p1	CLMcom-CCLM4–8-17	☑	☑	☑	☑	☑	☑
CCCma-CanESM2	r1i1p1	GERICS-REMO2015	☑	☑	☑	☑	☑	☑
CNRM-CERFACS-CNRM-CM5	r1i1p1	CLMcom-CCLM4–8-17	☑	☑	☑	☑	☑	☑
CNRM-CERFACS-CNRM-CM5	r1i1p1	SMHI-RCA4	☑	☑	☑	☑	☑	☑
CNRM-CERFACS-CNRM-CM5	r1i1p1	CNRM-ALADIN53	☑ ⚹	☑	☑	☑	☑⚹	☑
CNRM-CERFACS-CNRM-CM5	r1i1p1	CNRM-ALADIN63	☑ ⚹	☑ ⚹	☑ ⚹	☑ ⚹	☑ ⚹	☑⚹
CNRM-CERFACS-CNRM-CM5	r1i1p1	KNMI-RACMO22E	☑ ⚹	☑ ⚹	☑ ⚹	☑ ⚹	☑ ⚹	☑⚹
CNRM-CERFACS-CNRM-CM5	r1i1p1	GERICS-REMO2015	☑	☑	☑	☑	☑	☑
CNRM-CERFACS-CNRM-CM5	r1i1p1	DMI-HIRHAM5	☑	☑	☑	☑	☑	☑
CNRM-CERFACS-CNRM-CM5	r1i1p1	IPSL-WRF381P	☑	☑	☑	☑	☑	☑
ICHEC-EC-EARTH	r12i1p1	CLMcom-CCLM4–8-17	☑ ⚹	☑ ⚹	☑ ⚹	☑ ⚹	☑ ⚹	☑⚹
ICHEC-EC-EARTH	r12i1p1	CLMcom-ETH-COSMO-crCLIM-v1–1	☑	☑	☑	☑	☑	☑
ICHEC-EC-EARTH	r12i1p1	DMI-HIRHAM5	☑	☑	☑	☑	☑	☑
ICHEC-EC-EARTH	r12i1p1	KNMI-RACMO22E	☑ ⚹	☑ ⚹	☑ ⚹	☑ ⚹	☑ ⚹	☑⚹
ICHEC-EC-EARTH	r12i1p1	GERICS-REMO2015	☑ ⚹	☑ ⚹	☑ ⚹	☑ ⚹	☑ ⚹	☑⚹
ICHEC-EC-EARTH	r12i1p1	UHOH-WRF361H	☑	☑	☑		☑	
ICHEC-EC-EARTH	r1i1p1	DMI-HIRHAM5	☑	☑	☑	☑	☑	☑
ICHEC-EC-EARTH	r1i1p1	KNMI-RACMO22E	☑	☑	☑	☑	☑	☑
ICHEC-EC-EARTH	r3i1p1	DMI-HIRHAM5	☑ ⚹	☑ ⚹	☑ ⚹	☑ ⚹	☑ ⚹	☑⚹
ICHEC-EC-EARTH	r3i1p1	KNMI-RACMO22E	☑	☑	☑	☑	☑	☑
ICHEC-EC-EARTH	r1i1p1	SMHI-RCA4	☑	☑	☑	☑	☑	☑
ICHEC-EC-EARTH	r12i1p1	SMHI-RCA4	☑ ⚹	☑ ⚹	☑ ⚹	☑ ⚹	☑ ⚹	☑⚹
ICHEC-EC-EARTH	r3i1p1	SMHI-RCA4	☑	☑	☑	☑	☑	☑
MOHC-HadGEM2-ES	r1i1p1	CLMcom-CCLM4–8-17	☑	☑	☑	☑	☑	☑
MOHC-HadGEM2-ES	r1i1p1	DMI-HIRHAM5	☑	☑	☑	☑	☑	☑
MOHC-HadGEM2-ES	r1i1p1	KNMI-RACMO22E	☑ ⚹	☑ ⚹	☑ ⚹	☑ ⚹	☑ ⚹	☑⚹
MOHC-HadGEM2-ES	r1i1p1	SMHI-RCA4	☑ ⚹	☑ ⚹	☑ ⚹	☑ ⚹	☑ ⚹	☑⚹
MOHC-HadGEM2-ES	r1i1p1	GERICS-REMO2015	☑ ⚹	☑ ⚹	☑ ⚹	☑ ⚹	☑ ⚹	☑⚹
MOHC-HadGEM2-ES	r1i1p1	ICTP-RegCM4–6	☑ ⚹	☑ ⚹	☑ ⚹	☑ ⚹	☑ ⚹	☑⚹
MOHC-HadGEM2-ES	r1i1p1	UHOH-WRF361H	☑	☑	☑		☑	
MOHC-HadGEM2-ES	r1i1p1	IPSL-WRF381P	☑	☑	☑	☑	☑	☑
MOHC-HadGEM2-ES	r1i1p1	CNRM-ALADIN63	☑	☑	☑	☑	☑	☑
IPSL-IPSL-CM5A-MR	r1i1p1	SMHI-RCA4	☑	☑	☑	☑	☑	☑
IPSL-IPSL-CM5A-MR	r1i1p1	IPSL-WRF381P	☑	☑	☑	☑	☑	☑
IPSL-IPSL-CM5A-MR	r1i1p1	KNMI-RACMO22E	☑	☑	☑	☑	☑	☑
MIROC-MIROC5	r1i1p1	CLMcom-CCLM4–8-17	☑ ⚹	☑ ⚹	☑ ⚹	☑ ⚹	☑ ⚹	☑⚹
MIROC-MIROC5	r1i1p1	GERICS-REMO2015	☑ ⚹	☑ ⚹	☑ ⚹	☑ ⚹	☑ ⚹	☑⚹
MPI-M-MPI-ESM-LR	r1i1p1	CLMcom-CCLM4–8-17	☑ ⚹	☑ ⚹	☑ ⚹	☑	☑	☑⚹
MPI-M-MPI-ESM-LR	r1i1p1	KNMI-RACMO22E	☑	☑	☑	☑	☑	☑
MPI-M-MPI-ESM-LR	r1i1p1	SMHI-RCA4	☑	☑	☑	☑ ⚹	☑ ⚹	☑⚹
MPI-M-MPI-ESM-LR	r1i1p1	MPI-CSC-REMO2009	☑ ⚹	☑ ⚹	☑ ⚹	☑ ⚹	☑ ⚹	☑⚹
MPI-M-MPI-ESM-LR	r1i1p1	ICTP-RegCM4–6	☑ ⚹	☑ ⚹	☑ ⚹	☑	☑	☑
MPI-M-MPI-ESM-LR	r1i1p1	UHOH-WRF361H	☑ ⚹	☑ ⚹	☑ ⚹		☑	
MPI-M-MPI-ESM-LR	r1i1p1	CLMcom-ETH-COSMO-crCLIM-v1–1	☑	☑	☑	☑	☑	☑
MPI-M-MPI-ESM-LR	r2i1p1	MPI-CSC-REMO2009	☑ ⚹	☑ ⚹	☑ ⚹	☑ ⚹	☑ ⚹	☑⚹
MPI-M-MPI-ESM-LR	r2i1p1	CLMcom-ETH-COSMO-crCLIM-v1–1	☑	☑	☑	☑	☑	☑
MPI-M-MPI-ESM-LR	r3i1p1	SMHI-RCA4	☑⚹	☑⚹	☑ ⚹	☑	☑	☑
MPI-M-MPI-ESM-LR	r3i1p1	GERICS-REMO2015	☑⚹	☑⚹	☑ ⚹	☑	☑	☑
MPI-M-MPI-ESM-LR	r3i1p1	CLMcom-ETH-COSMO-crCLIM-v1–1	☑	☑	☑	☑	☑	☑
NCC-NorESM1-M	r1i1p1	DMI-HIRHAM5	☑	☑	☑	☑	☑	☑
NCC-NorESM1-M	r1i1p1	KNMI-RACMO22E	☑	☑	☑	☑	☑	☑
NCC-NorESM1-M	r1i1p1	GERICS-REMO2015	☑	☑	☑	☑ ⚹	☑ ⚹	☑⚹
NCC-NorESM1-M	r1i1p1	SMHI-RCA4	☑	☑	☑	☑ ⚹	☑ ⚹	☑⚹
NCC-NorESM1-M	r1i1p1	IPSL-WRF381P	☑	☑	☑	☑	☑	☑
NCC-NorESM1-M	r1i1p1	CLMcom-ETH-COSMO-crCLIM-v1–1	☑	☑	☑	☑	☑	☑

Note. tas = atmospheric 2 m temperature; tasmin = minimum 2 m daily temperature; tasmax = maximum 2 m daily temperature; pr = precipitation; q = specific humidity, rsds = surface downwelling shortwave radiation. This list is relevant for all historical and rcp85 and RCM2.6 simulations (☑ rcp8.5, ⚹ = rcp2.6).

Table 2
CMIP5 Models and Their Corresponding Variant Label Used for This Report

CMIP5	Variant	tas	tasmax	tasmin	q	pr	rsds
CanESM2	r1i1p1	☑	☑	☑	☑ ✲	☑	☑✲
CNRM-CM5	r1i1p1	☑✲	☑✲	☑✲	☑ ✲	☑✲	☑✲
EC-EARTH	r12i1p1	☑✲	☑✲	☑✲		☑✲	☑
EC-EARTH	r3i1p1	☑	☑	☑		☑	
EC-EARTH	r1i1p1	☑	☑	☑		☑	☑
HadGEM2-ES	r1i1p1	☑✲	☑✲	☑✲	☑ ✲	☑✲	☑✲
IPSL-CM5A-MR	r1i1p1	☑	☑	☑	☑ ✲	☑	☑✲
MIROC5	r1i1p1	☑✲	☑✲	☑✲	☑ ✲	☑✲	☑✲
MPI-ESM-LR	r1i1p1	☑✲	☑✲	☑✲		☑✲	☑✲
MPI-ESM-LR	r2i1p1	☑✲	☑✲	☑✲		☑✲	☑✲
MPI-ESM-LR	r3i1p1	☑	☑	☑		☑	☑✲
NorESM1-M	r1i1p1	☑✲	☑✲	☑✲	☑	☑✲	☑✲

Note. ☑ rcp8.5, ✲ = rcp2.6.

RCMs. The details about model availability for each of the variables and indices for both the RCP8.5 and RCP2.6 scenarios are reported in Table 1.

The reader is also referred to Vautard et al. (2020) for model references. Also note that not all variables are available for all models, especially in the RCP2.6 projections. The second ensemble used for comparison consists of 12 GCM simulations (with 8 different GCMs) from CMIP5 (Taylor et al., 2012). These are limited to those simulations used as boundary conditions for the RCM ensemble assessed here (see Table 2). As a third ensemble, 12 simulations from CMIP6 (Eyring et al., 2016) are analyzed and intercompared over the European area.

The CMIP6 ensemble is reported in Table 3 and is based on the availability of data on the Earth System Grid Federation (ESGF) archive at the time when the analysis was completed. EURO-CORDEX and CMIP5 simulations share the same forcing scenarios, that is, RCP8.5 and RCP2.6 (Representative Concentration Pathway; see Moss et al., 2010) while the CMIP6 simulations use the SSP126 and SSP585 scenarios (Shared Socio-Economic Pathways, Riahi et al., 2017). The time slices used to compute the climate change signal with respect to the historical period 1981–2010 are 2041–2070 for the mid-future and 2071–2100 for the far future (end of century). The EURO-CORDEX ensemble results are presented on a regular 0.11° grid, the CMIP5 GCMs on a 2° grid and the CMIP6 on a 1° grid. These grids were chosen to be representative of the resolution of each ensemble. The robustness of the simulated changes of the three ensembles was evaluated by means of a significance test based on the dependent samples of a two-sided Student's t test.

2.1.1. Extreme and Impact-Oriented Climate Indices

As in Vautard et al. (2020), we use here a set of 13 extreme and impact-oriented indices described in Table 4, which characterize a number of potential influences on different sectors. The description of the indices is

Table 3
CMIP6 Models and Their Corresponding Variant Label Used for This Report

CMIP6	Variant	tas	tasmax	tasmin	q	pr	rsds
BCC-CSM2-MR	r1i1p1f1	☑ ✲	☑ ✲	☑ ✲	☑ ✲	☑✲	☑✲
CNRM-CM6–1	r1i1p1f2	☑ ✲	☑ ✲	☑ ✲	☑	☑✲	☑✲
CNRM-ESM 2–1	r1i1p1f2	☑ ✲	☑ ✲	☑ ✲	☑ ✲	☑✲	☑✲
CanESM5	r1i1p1f1	☑ ✲	☑ ✲	☑ ✲	☑ ✲	☑✲	☑✲
EC-Earth3	r1i1p1f1	☑ ✲	☑ ✲	☑ ✲	☑ ✲	☑✲	☑✲
EC-Earth3-Veg	r1i1p1f1	☑ ✲	☑ ✲	☑ ✲	☑ ✲	☑✲	☑✲
GFDL-CM4	r1i1p1f1	☑	☑	☑	☑	☑	☑
IPSL-CM6A-LR	r1i1p1f1	☑ ✲	☑ ✲	☑ ✲	☑	☑✲	☑✲
MIROC6	r1i1p1f1	☑ ✲	☑ ✲	☑ ✲		☑✲	☑✲
MRI-ESM 2–0	r1i1p1f1	☑ ✲	☑ ✲	☑ ✲	☑ ✲	☑✲	☑✲
NESM3	r1i1p1f1	☑ ✲	☑ ✲	☑ ✲		☑✲	☑✲
UKESM1–0-LL	r1i1p1f2	☑ ✲	☑ ✲	☑ ✲	☑ ✲	☑✲	☑✲

Note. ☑ = ssp585, ✲ = ssp126.

Table 4
Diagnostics and Climate Indices Used in This Study

Variable	Analyzed period	Description
Daily mean temperature (TAS)	Year, DJF, JJA, SON, MAM	Yearly and seasonal mean temperature from daily mean temperature, °C
Daily max temperature (TASMAX)	Year, DJF, JJA, SON, MAM	Yearly or seasonal mean of daily maximum temperature, °C
Daily min temperature (TASMIN)	Year, DJF, JJA, SON, MAM	Yearly or seasonal mean of daily minimum temperature, °C
TXx (yearly max temperature)	Year	Yearly maximum of daily maximum temperature, °C
TNn (yearly min temperature)	Year	Yearly minimum of daily minimum temperature, °C
#days/year TX > 35°C (TX35)	Year	Number of days per year with maximum temperature over 35°C
#days/year TX > 40°C (TX40)	Year	Number of days per year with maximum temperature over 40°C
#days wet bulb globe temperature >31°C (WBGTs31)	Year	Number of days per year with wet bulb globe temperature (WBGT) larger than 31°C
#Frost days/year (FD)	Year	Number of days per year with minimum temperature below 0°C
Length of frost-free period (LFFP)	Year	Maximum continuous number of days per year where daily minimum temperature is above 0°C (units = days). (McCabe et al., 2015)
Growing degree days >5°C (GDD)	Year	The accumulated sum of the difference between daily mean temperature and the threshold (5°C) (when higher than the threshold) over the April–September months (units = degree days) (McCabe et al., 2015; Ruosteenoja et al., 2016; Spinoni et al., 2015)
Heating degree day >15.5 (HDD)	Year	Heating degree days, threshold (Tb) = 15.5°C, following Spinoni et al. (2015), which uses the mean (TM), maximum (TX) and minimum (TN) daily temperature as follows (units = degree days): $HDD_i = \begin{cases} T_b - T_M \\ \frac{T_b - T_N}{2} - \frac{T_X - T_b}{4} \\ \frac{T_X - T_N}{4} \\ 0 \end{cases} \quad if \begin{cases} T_X \le T_b \\ T_M \le T_b < T_X \\ T_N \le T_b < T_M \\ T_N \ge T_b \end{cases}$ Then $HDD = \sum_{i=1}^{365} HDD_i$ We use all months of the year
Cooling degree day >22°C (CDD)	Year	Cooling degree days, threshold (Tb) = 22°C, following Spinoni et al. (2015), which uses the mean (TM), maximum (TX) and minimum (TN) daily temperature as follows (units = degree days): $CDD_i = \begin{cases} 0 \\ \frac{T_X - T_b}{4} \\ \frac{T_X - T_b}{2} - \frac{T_b - T_N}{4} \\ T_M - T_b \end{cases} \quad if \begin{cases} T_X \le T_b \\ T_M \le T_b < T_X \\ T_N \le T_b < T_M \\ T_N \ge T_b \end{cases}$ Then $CDD = \sum_{i=1}^{365} CDD_i$ We use all months of the year
Daily precipitation amount (PR)	Year, DJF, JJA, SON, MAM	
SDII	Year	Simple Daily Intensity Index (units = mm/day)
RX1day	Year	Highest 1-day precipitation amount (units = mm/day)
RX5day	Year	Highest 5-days precipitation amount (units = mm/5 days)
P99	Year	Days with RR > 99th percentile of daily amounts (extremely wet days). Units: days
CDD_pr	Year	Mean consecutive dry days per year. Units = number of days
Drought frequency (DF)	Year	Drought frequency change per decade, based on a Standardized Precipitation Index (SPI) computed for a 6 month accumulation period
Downward surface solar radiation (RSDS)	Year	rsds variable

provided in Vautard et al. (2020) and references therein, to which we refer for more detailed information. However, a few additional indices are used here: the Simple Daily Intensity Index (SDII) and the Highest 5 day precipitation amount (RX5day). Only for the daily wet bulb globe temperature (WBGT) index, data are bias-corrected for each climate model on each grid point and each month of the year individually

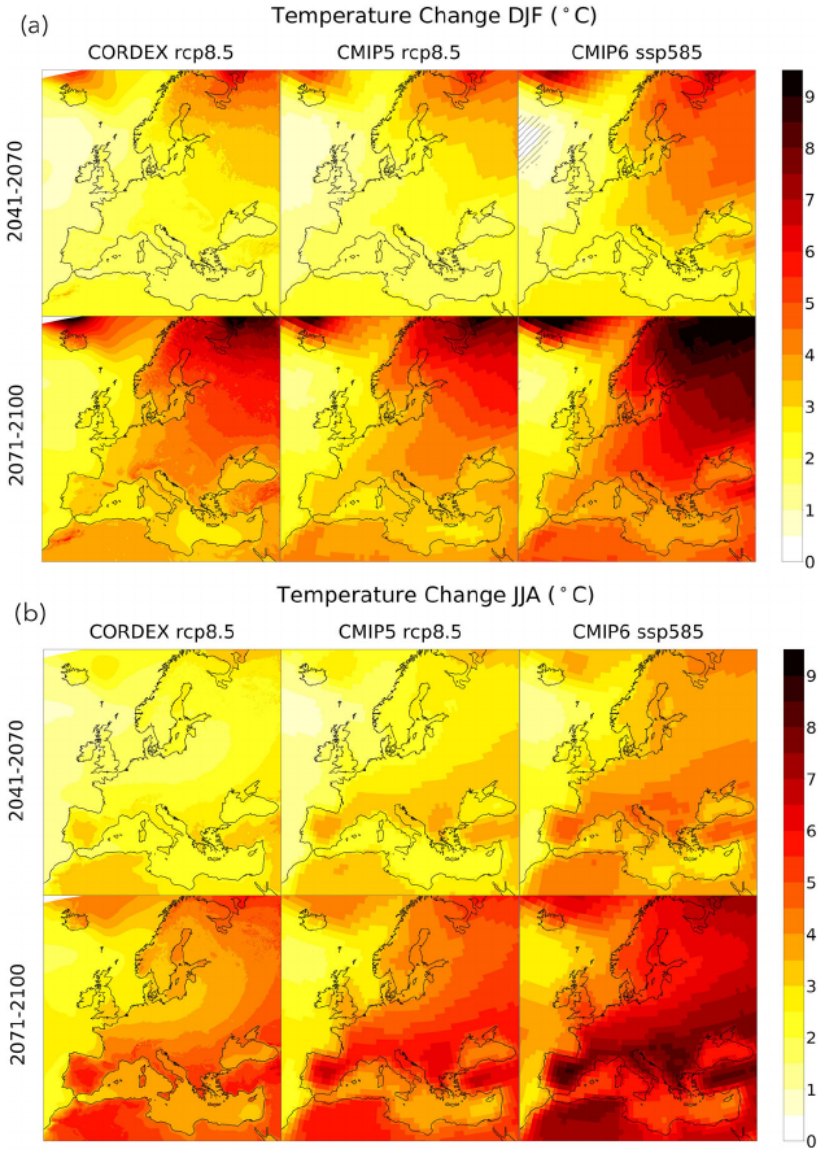

Figure 1. Seasonal mean temperature ensemble mean changes (DJF, a; and JJA, b) for EURO -CORDEX (55 simulations), CMIP5 (12 simulations), and CMIP6 (12 simulations) for 2041–2070 (mid-future) and 2071–2100 (far future) relative to 1981–2010 (units: degrees). Dashed lines cover areas where changes are not significant at the 95% confidence level (Student's t test).

using the quantile delta mapping approach described by Cannon et al. (2015). We use ERA5 as reference data set and 1981–2010 as reference period.

3. Results

Here climate change signals are compared for the mid-century (2041–2070) and end of century (or far future, 2071–2100) time slices under the RCP8.5 scenario. An identical analysis is reported for the RCP2.6 scenario for the box plot results and in the supplementary material for the remaining analysis. The mean seasonal changes are shown for mean, maximum and minimum temperature and precipitation over the whole European domain and box plots are used to summarize the results for the Northern European (NEU), Central European (CEU), and Mediterranean (MED) regions, following the definition in Iturbide et al. (2020). Values of change are shown for the median, the 25th, and 75th percentiles, together with the 5th and 95th

Figure 2. Summer (JJA) and winter (DJF) daily precipitation (units = percentage) and temperature (mean temperature *tas*, minimum temperature *tasmin*, and maximum temperature *tasmax*, units = degrees) changes of 2041–2070 (mid-) and 2071–2100 (far) relative to 1981–2010 for the three European SREX regions (Northern Europe, Central Europe, and Mediterranean region). The colors indicate different ensembles (CORDEX [55 simulations], CMIP5 [12 simulations] and CMIP6 [12 simulations]) under different scenarios (rcp85, rcp26, ssp585, and ssp126). Colored bars represent the model spread between the 25th and 75th percentiles, while the black bars indicate the 5th, the 50th, and 95th percentiles.

percentiles. Similarly, all the temperature and heat indices as well as the wet and dry indicators and radiation are shown as spatial change plots over Europe, while box plots are provided for the hazard indices.

3.1. Mean Temperature

Figure 1 shows the seasonal mean temperature change for DJF (winter) and JJA (summer), the mid-future and far future time slices in the RCP8.5 projections and the EURO-CORDEX, CMIP5 and CMIP6 ensembles.

In DJF all three ensembles show a well-known temperature change gradient, with the largest warming in the north and northeast and the weakest warming in the southwest and over the Atlantic. This warming pattern is to a large extent a result of the Arctic warming amplification, for which an important contribution is sea ice loss as well as the reduction of continental snow cover over vast northern areas leading to the snow albedo feedback (e.g., Dai et al., 2019; Walsh, 2014). Another contribution has been identified in the increased intrusion of low pressure systems, as explained in AMAP (2017). Figure 1 also shows differences between the ensembles in the amplitude of the change. In general, the CMIP6 ensemble shows a much stronger warming compared to the other two CMIP5-based ensembles, except for some areas over the Atlantic in winter. Another difference relates to the RCM ensemble which, in addition to more fine-scale

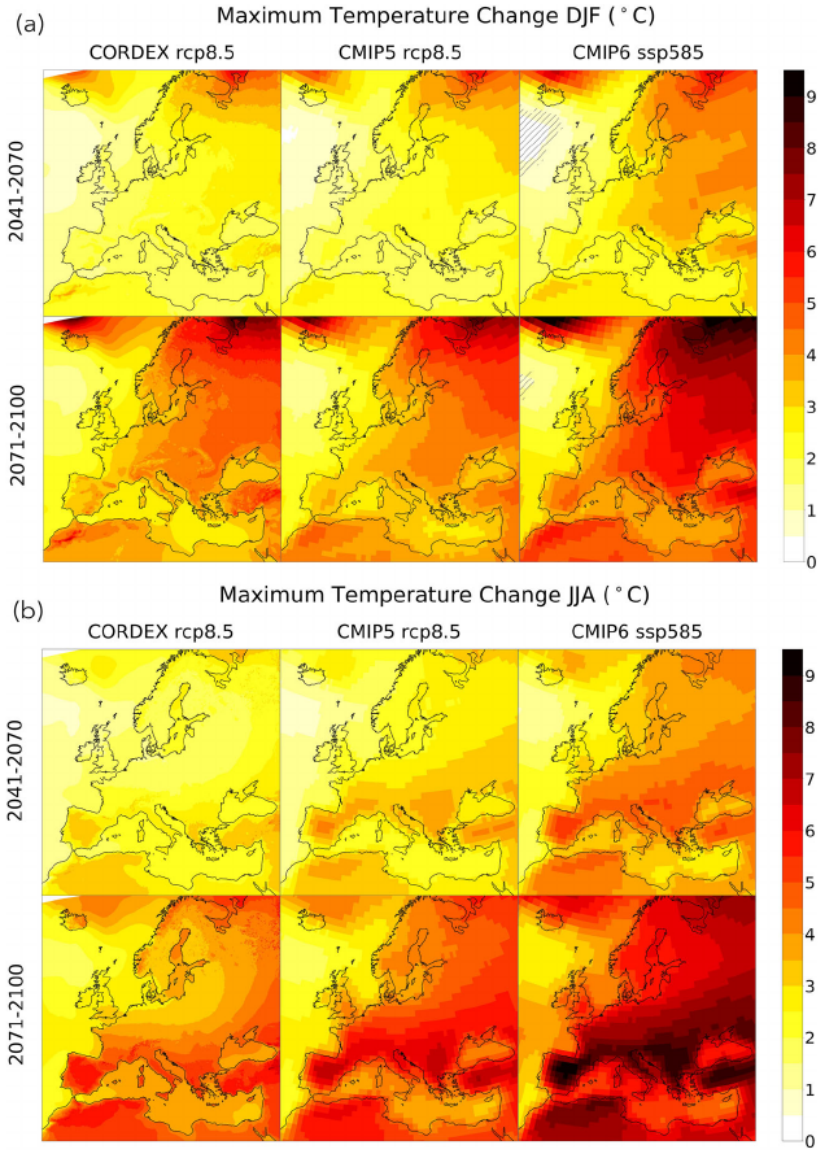

Figure 3. As in Figure 1 for seasonal maximum temperature ensemble changes (DJF, a; and JJA, b) (units: degrees). Dashed lines cover areas where changes are not significant at the 95% confidence level (Student's t test).

details, shows weaker warming over large parts of the continent compared to the driving CMIP5-GCMs. This is in line, for example, with results from Sørland et al. (2018).

Figure 2 shows the box plot for the NEU and CEU regions of the area average change for each ensemble with colored bars representing the model spread between the 25th and 75th percentiles, while the black bars indicate the 5th, 50th, and 95th percentiles A projected median warming in winter of 4.5°C (2.5°C) is found for the RCM and CMIP5 ensemble in the far (mid-) future time slices, respectively, reaching values of 6°C (3.5°C) and 5.5°C (3.8°C) for CMIP6. Over the MED region a smaller DJF warming is projected, with slightly less than 3.5°C (2°C), for both EURO-CORDEX and CMIP5, and 4.5°C (2.5°C) and 6°C (4°C) for CMIP6. The projections for the 90% interval (range between the 5th and 95th percentiles) are generally less than 1.5° for the EURO-CORDEX and CMIP5 ensembles in all regions, and reach ~3° in NEU and MED for CMIP6.

The JJA warming has its maximum signal over the Mediterranean land regions with values above 4°C (2.5°C), 4.5°C (2.5°C), and 6.5°C (3.5°C) for RCM, CMIP5 and CMIP6, respectively, in the far (mid-) future (Figure 2). This result, which is in line with previous analyses (e.g., Giorgi & Coppola, 2010; Giorgi &

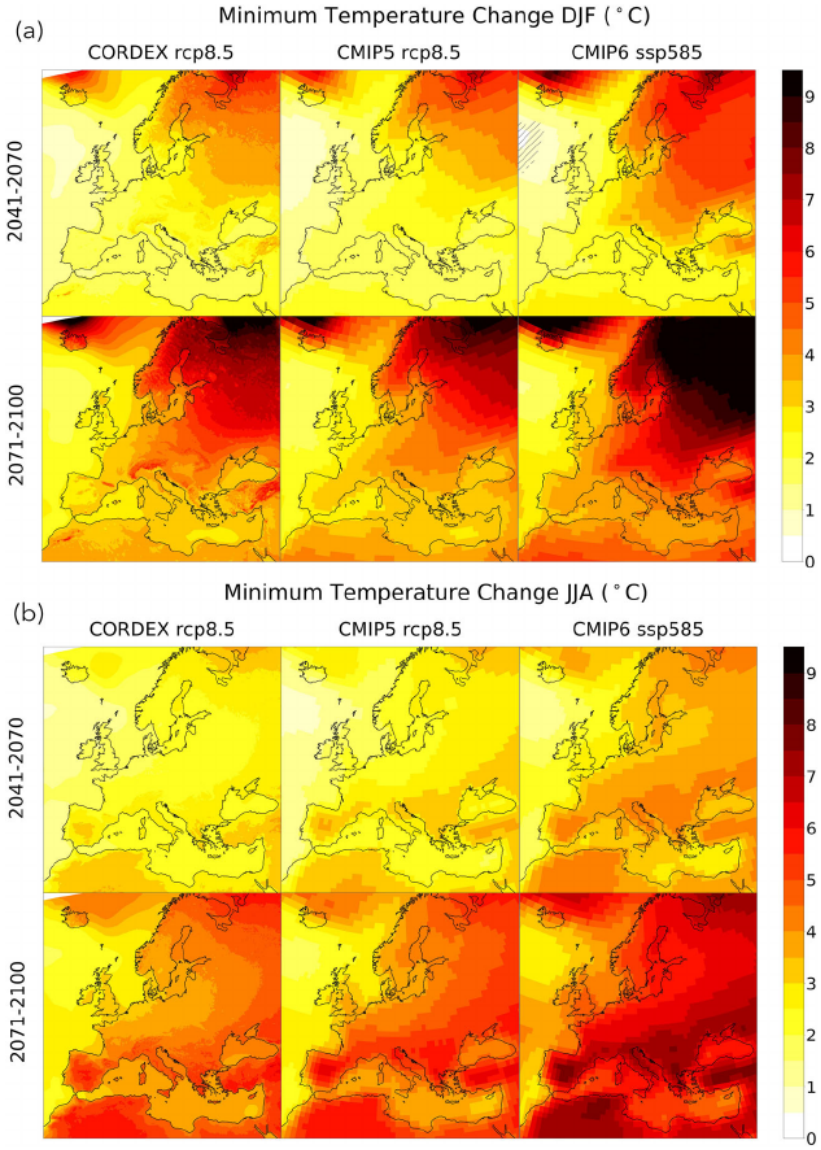

Figure 4. As in Figure 1 for seasonal minimum temperature ensemble changes (DJF, a; and JJA, b) (units: degrees). Dashed lines cover areas where changes are not significant at the 95% confidence level (Student's t test).

Lionello, 2008) is likely connected with a marked decrease in spring and summer precipitation (as shown on Figure 3), increased soil drying and decreased cloud cover.

The NEU and CEU regions warm less in summer, with values in the far (mid-) future of 3.5°C (2°C), 3.6°C (2.3°C), 5.8°C (3°C), and 3.5°C (2°C), 4°C (2.3°C), and 6°C (3.4°C), respectively, for the EURO-CORDEX, CMIP5 and CMIP6 ensemble. The spread connected to the projections is lower for the first two ensembles compared to the CMIP6. The RCP2.6 scenario has a general warming between 1°C and 2.5°C for both seasons and for the three ensembles, with CMIP6 being at the upper end of the distribution. In summary, the warming projected by the EURO-CORDEX ensemble is comparable with that in the CMIP5 ensemble in DJF, while it is about 0.5° lower on average in JJA.

These findings confirm previous results based on a more sophisticated ANOVA analysis (Christensen et al., 2019; Déqué et al., 2007; Evin et al., 2019) from which most of the temperature change signal is largely influenced by the choice of GCM, while the RCM mostly dominates the change pattern in regions of complex topography, sea ice, soil moisture or snow. The difference between the RCM and GCM warming during

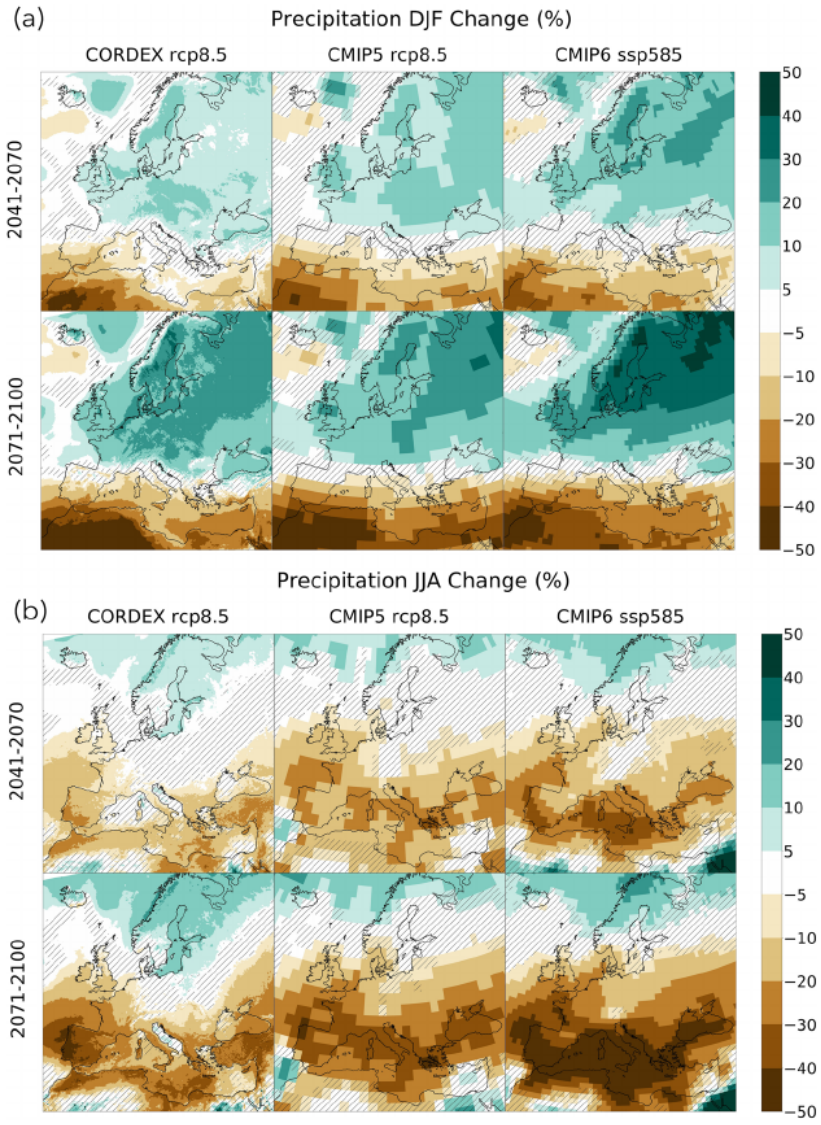

Figure 5. As in Figure 1 for seasonal precipitation ensemble changes (DJF, a; and JJA, b) (units: percentage). Dashed lines cover areas where changes are not significant at the 95% confidence level (Student's t test).

summer also confirms the finding of Sørland et al. (2018) and Boé et al. (2020), that is, that CMIP5 GCMs warm notably more than RCMs even on a pair by pair basis (not shown). Possible explanations for this result are multiple. Some studies have at least partially attributed it to the lack of aerosol forcing in the RCMs, since aerosol concentrations over Europe are expected to decrease in the future as a result of stricter emission control measures (Boé et al., 2020; Gutiérrez et al., 2019; Nabat et al., 2020). Other reasons can be related to clouds (Bartók et al., 2017) or differences in the representation of plant physiological effects (Schwingshackl et al., 2019). The consistently higher warming values of the CMIP6 ensemble, along with the much higher uncertainty spread, is in line with the higher equilibrium climate sensitivity (ECS) of some of the members of CMIP6 (Forster et al., 2020; Zelinka et al., 2020), whose origin remains unclear and is under investigation.

Maximum (TXx) and minimum (TNn) temperature seasonal projections are shown in Figures 3 and 4, while the median and percentile values are reported as box plots in Figure 2. Both variables show a similar behavior as the mean temperature. Maximum winter warming occurs in the NEU and CEU regions, with a change of the TXx median value of about 4°C (2.5°C) (EURO-CORDEX and CMIP5) and 5.3°C (3–3.5°C)

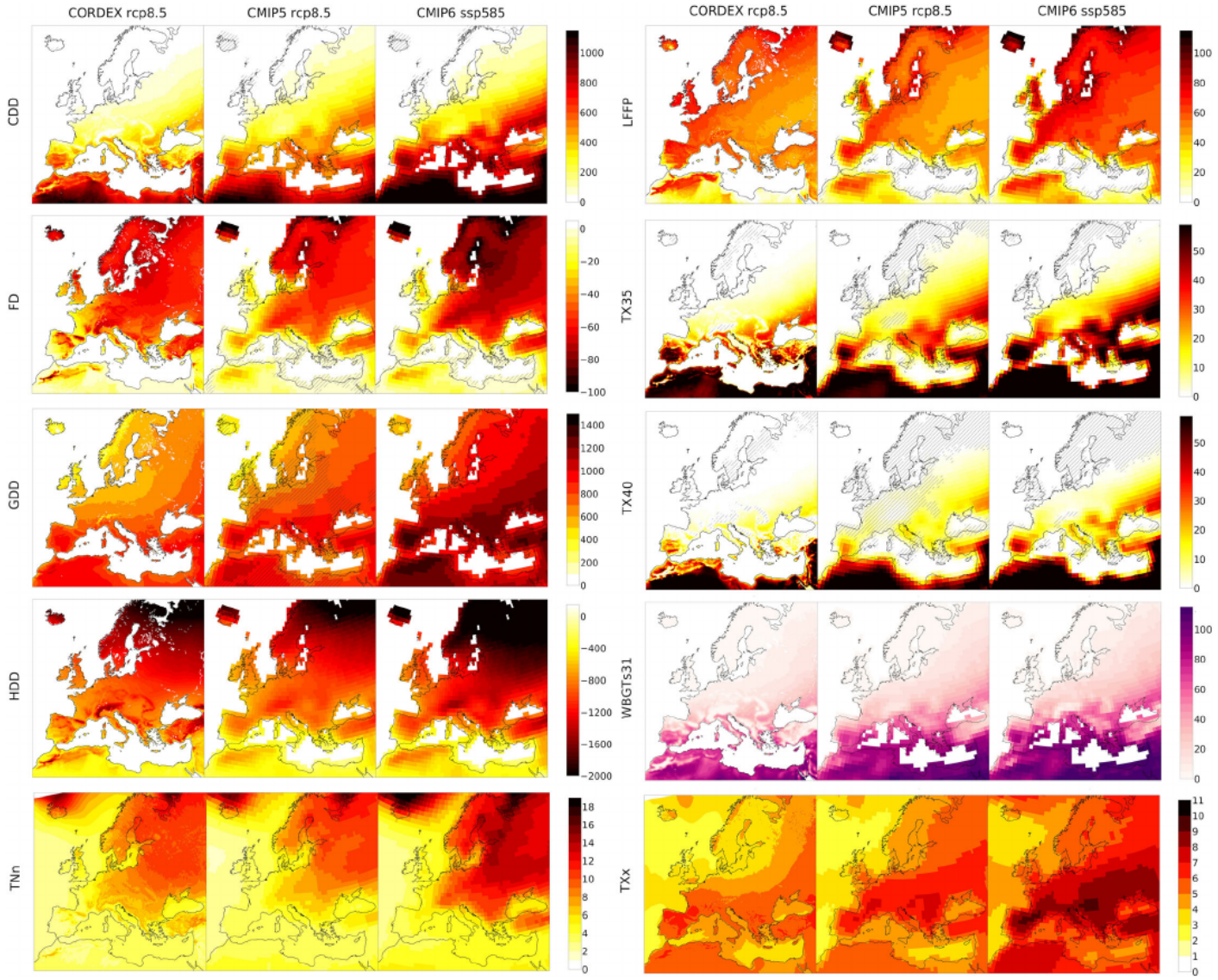

Figure 6. Changes of the following indices: Cooling degree days >22°C change (CDD, units: degree days derived over the whole year), frost days (FD, units: number of days per year), growing degree days >5°C (GDD, units: degree days), heating degree days (HDD, units: degree days), length of frost-free period change (LFFP, units: days), number of days per year with maximum temperature over 35°C and 40°C (TX30 and TX40, units: days per year), and number of yearly events with wet bulb globe temperature greater than 31°C (WBGTs31, units: number of events per year). Results are shown for EUROuro-CORDEX (55 simulations), CMIP5 (12 simulations), and CMIP6 (12 simulations) for 2071–2100 (Far future) relative to 1981–2010. Dashed lines cover areas where changes are not significant at the 95% confidence level (Student's t test).

(CMIP6) at the far (mid-) century. In winter, TNn shows greater warming in NEU and CEU compared to TNx about 4.5°C (2.5°C) for EURO-CORDEX and CMIP5 and 7°C (4°C) and 5.5°C (4.5°C) for CMIP6 far (mid-) century, probably due to the snow albedo feedback. For the MED region, the TXx and TNx warming in DJF has values of 3.5°C (2°C) for the RCM and CMIP5 ensembles and 4.5°C (2.5°C) for the CMIP6 ensemble far (mid-) century time slice, with a very limited model spread (about 1°) for all the three ensembles probably due to the lower temperature variability over the ocean compared to the land. In summer, the changes in maximum and minimum temperature in the three European sub-regions have similar values (Figure 2). For NEU the median change value for both variables by the far (mid-) 2100 are around 3.5°C (2°C) for EURO-CORDEX and CMIP5 and 6°C (3°C) for CMIP6; TNn for CEU has a 3.5°C (2°C) median increase for the regional ensemble, while the GCM ensembles show stronger warming by 1° (0.5°) for CMIP5 and 2° for CMIP6 for the far (mid-) century time slice. TXx shows the same behavior. In

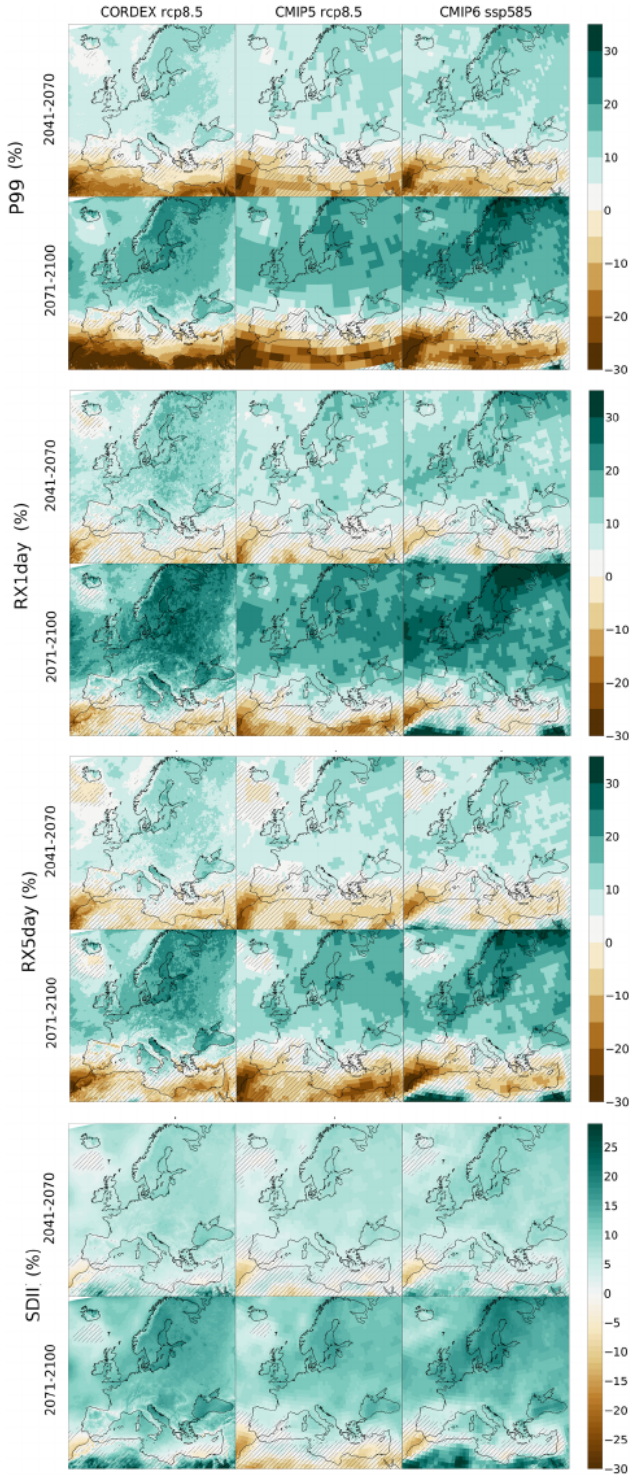

Figure 7. As in Figure 1 for annual changes of the following indices: the yearly 99th percentile of daily precipitation ensemble changes (units: percentage), the maximum 1 day precipitation changes (RX1day) (units: percentage), the maximum 5 day precipitation changes (RX5day) (units: percentage), and the simple daily intensity precipitation index (SDII) (units: percentage). Dashed lines cover areas where changes are not significant at the 95% confidence level (Student's t test).

the MED region, TXx warms by about 0.5° more than TNn, with median values of 4.5°C (2.5°C), 5°C (2.7°C), and 6.5°C (3.7°C) for CORDEX, CMIP5 and CMIP6 by the far (mid-) future, respectively.

3.2. Mean Precipitation

Figure 5 shows the seasonal mean precipitation change in percent of reference values for DJF and JJA. The well-known north-south dipole is evident, with positive changes in the northern part of the domain and negative changes in the southern part. The zero-change line is positioned in the southernmost location during winter over the Pyrenees, Alpine and Balkan Mountains, and shifts northward during the spring and summer season when it reaches the northernmost position placed over central eastern Europe and southern Scandinavia (Giorgi & Coppola, 2007).

For NEU and CEU in DJF, the EURO-CORDEX ensemble shows a median precipitation increase for the 2071–2100 (2041–2070) time slice of 15% (5%) and 20% (10%), respectively, with the smallest inter-model spread for the NEU and the largest over the CEU in all ensembles (see Figure 2). Change patterns are similar in the CMIP5 ensemble, with an amplitude of the spread about doubled over NEU and halved over CEU compared to the EURO-CORDEX one. The CMIP6 ensemble exhibits a 25% (15%) and 22% (12%) median value of increase over the two regions, respectively, and a spread similar to the CMIP5 one in NEU but greater in CEU, and lower than the RCM spread. In the Mediterranean region the three ensembles project a median negative DJF precipitation change slightly above 10% (5%), with a wider spread for the RCMs.

For the summer, over the NEU the three ensembles project an increase of about 5% for both the mid-future and far future time slices and for both the RCP8.5 and RCP2.6 scenarios, with a larger spread for the far future time slice compared to the mid-century one and a range of 20% between the 5th and 95th percentiles. Again, the RCM ensemble shows the widest spread. In CEU and MED all ensembles agree on negative changes of precipitation for far (mid-) century, spanning the range of −7% (4%) for EURO-CORDEX to −20% (−10%) for CMIP6 over CEU and from −22% (−10%) to −32% (−20%) in the Mediterranean. In all cases the CMIP5 ensemble has intermediate values between the EURO-CORDEX and CMIP6 ones. For the MED region far future projections, the range between the 5th and 95th percentiles is roughly 40% in the RCM ensemble and slightly lower (35%) for both CMIP ensembles.

3.3. Temperature Indices

3.3.1. Hot Extremes

Extremely hot days, as characterized by a daily maximum temperature larger than 35°C or 40°C, have a well-marked increasing frequency for RCP8.5/SSP585, particularly in regions where their occurrence is already significant in the reference period (see Vautard et al., 2020). In Southern Spain and low-lying areas of Italy and the Balkans, the number of days (35°C/40°C) is robustly projected to increase by more than 30 days/10 days in the mid-century and 50 days/20 days for the end of the century (Figure 6). This may have important impacts on agriculture and health, as these are typical critical thresholds above which these sectors are impacted.

3.3.2. WBGT

Humid heat, as characterized by the WBGT index, is projected to increase in large parts of Europe as indicated by the number of days during which

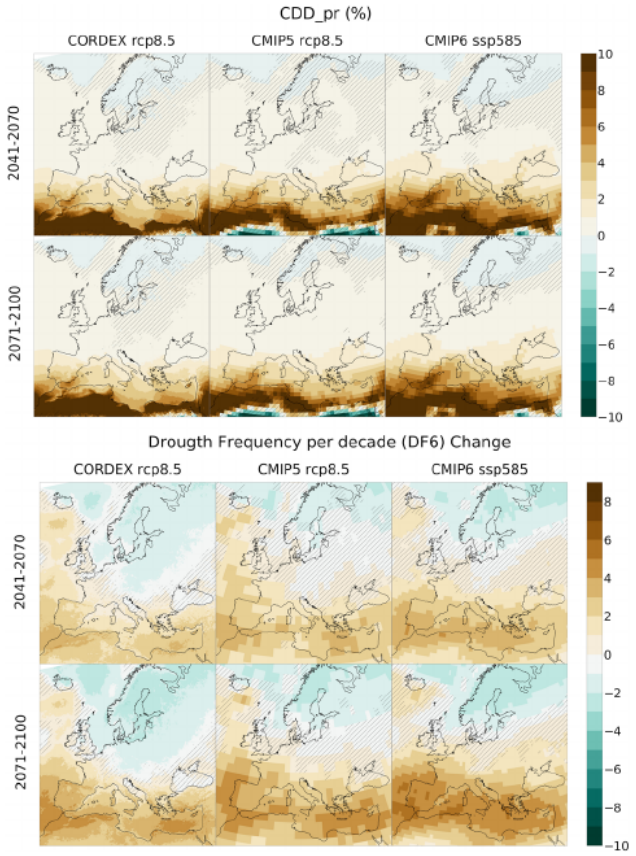

Figure 8. As in Figure 1 for changes of the consecutive dry day index (CDD, units: days) and of the Drought frequency per decade, based on a SPI-6 months (DF6, units: events per decade). Dashed lines cover areas where changes are not significant at the 95% confidence level (Student's t test).

WBGT exceeds 31°C, a danger threshold for which impacts and reduction of productivity are expected for outdoor activities (Figure 6). The EURO-CORDEX ensemble shows an increase of more than 30 days in low-lying, coastal or near-coastal areas of Southern Europe (e.g., Andalucia, Po Valley, lower Rhone and Garonne Valleys, coastal areas of Greece and Turkey, plains near the Black Sea). The number of days above the danger threshold is projected to almost double in the far future projection (see Vautard et al., 2020). In contrast to EURO-CORDEX, the WBGT signal is spread throughout Europe much more evenly in CMIP5 and CMIP6, highlighting the beneficial effects of improved orography resolution in RCM simulations compared to GCMs. The patterns in CMIP5 and CMIP6 are consistent, both showing large increases of the number of days with WBGT exceeding 31°C. Note that WBGT exceedances exhibit a cold bias in RCMs for current climate conditions (Vautard et al., 2020) and absolute changes in the number of days with WBGT exceeding 31°C should thus be treated cautiously.

3.3.3. Cooling Degree Days >22°C

Cooling degree days, which measure the energy demand for cooling are projected to strongly increase in several European regions. For the southernmost Mediterranean areas, we note approximately a doubling of the number of consecutive dry days (CDDs) by the mid-century and tripling by the end of the century compared to the present-day reference value (see Vautard et al., 2020), with a large spread among the ensembles (EURO-CORDEX showing lower values than CMIP5 and CMIP6). Again, we note that CMIP5 and CMIP6 exhibit reduced regional orographic details than EURO-CORDEX. Large increases in CDD are also expected by the end of century in Central Europe, while Scandinavia only shows a limited increase.

3.3.4. Growing Degree Days >5°C and Length of Frost-Free Period

The GDD index, which is linked to plant phenology and growing season length, is projected to increase across Europe, with a north-south gradient and significant differences between the ensembles. EURO-CORDEX and CMIP5 have a consistent change signal, while CMIP6 has a signal about 1.5 times larger than CMIP5. The GDD index is sensitive to spring and summer temperatures, and therefore its pattern is correlated to the temperature change pattern in these seasons.

By contrast, the LFFP index, which is mostly sensitive to winter temperature changes, has a different change pattern. It increases more in Northern Europe (40–70 days for mid-century and 60–100 days for the end of century) than in Southern Europe (15–30 days and 20–40 days) for RCP8.5, with a rather homogeneous spatial pattern, except in a few scattered areas such as along southwestern coasts of the Iberian Peninsula where frost days are almost absent. Again, the EURO-CORDEX and CMIP5 ensembles show rather similar changes while CMIP6 gives a larger increase. Note that, along the coastlines, the GCMs may be inaccurate and mix sea temperatures with land temperatures into a smoother pattern, hence the smaller increase.

3.3.5. Frost Days

Frost days relevant for both agriculture and energy, are projected to become much less frequent in the RCP8.5 Scenario. Their number varies in the reference period from about 150–250 days in Northern Europe to almost none in Southwestern Europe (see Vautard et al., 2020). For RCP8.5, in the mid-century, the decrease in frost days number is about 20–40 days (with a doubled reduction in CMIP6 in Northern and Central Europe), and at the end of the century, frost days are reduced by 50–60 days.

3.4. Wet and Dry Extremes

3.4.1. Precipitation 99th Percentile, SDII, RX1day, and RX5day

Figure 7 shows the extreme precipitation indices P99 (often connected with the pluvial flooding hazard), RX1day, RX5day and the precipitation intensity index SDII for the mid-future and far future time slices in the RCP8.5 scenario. All three indices for all the RCM and GCM ensembles show an increase in extreme

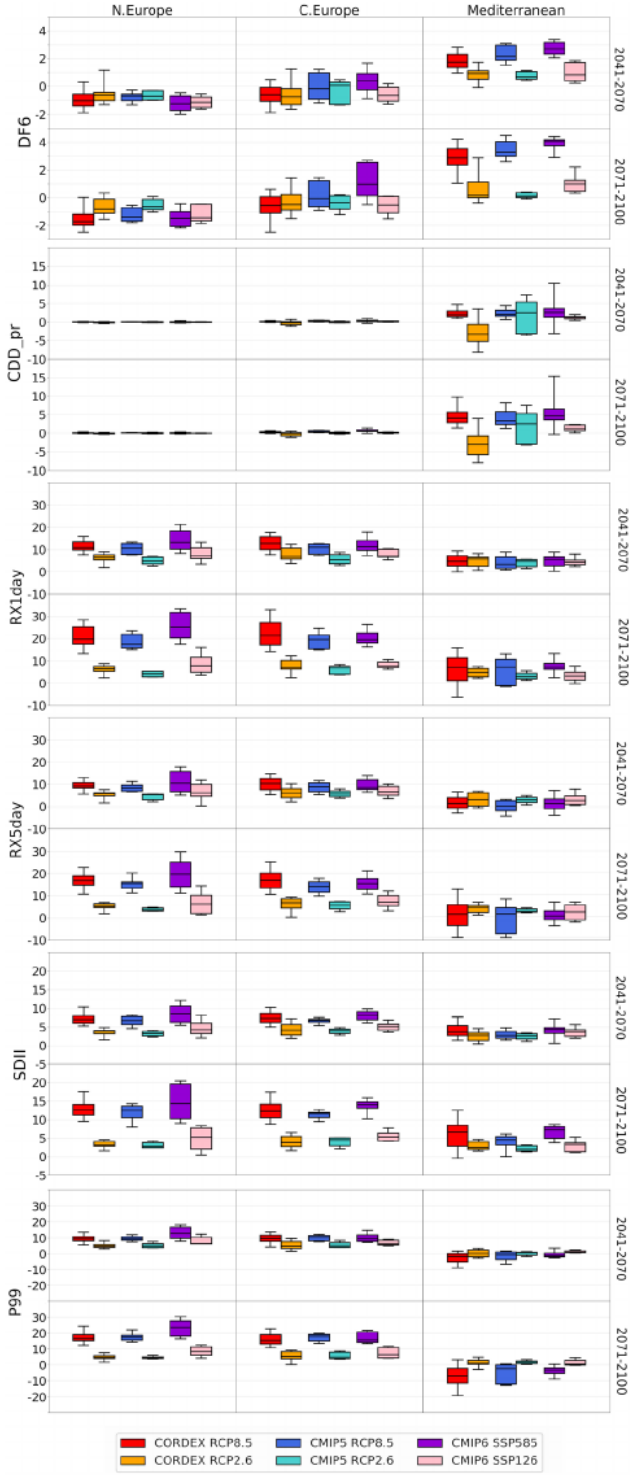

Figure 9. As in Figure 2 for the following indices: the Drought Frequency (DF6, units = events per decade), the number of consecutive dry days change (CDD, units = days), the Maximum 1 day precipitation changes (RX1day, units: percentage), the Maximum 5 day precipitation changes (RX5day, units: percentage), and the surface downwelling shortwave radiation (units: W/m^2).

precipitation events, with a maximum by the far (mid-) century above the 20% (10%) median increase over the European continental region and Scandinavia (Figure 9 box plot). The most intense changes are shown by the EURO-CORDEX ensemble over the CEU and MED regions, while the CMIP6 ensemble shows the largest increases in the northeast uppermost corner of the NEU region.

The Rx1day extreme index exhibits the strongest positive change among the three indices, with only less than 5% non-significant negative changes limited to the Gibraltar Strait, Pyrenees, Morocco coasts and the Peloponnesus in Greece. Due to the higher resolution, the EURO-CORDEX ensemble indicates a pronounced increase in extreme 1 day precipitation over the Padania plain in Italy and in Tuscany. The land-sea contrast is quite evident between the Tyrrhenian and Adriatic seas and the Italian peninsula, with more extreme values over the ocean and in particular a maximum over the northernmost part of the Adriatic Sea where the Venice lagoon is located.

A minimum of the daily maximum precipitation increase (RX1day) is evident over all the European mountains, such as the Pyrenees, the Alps, the Apennines, the Carpathians and the Norwegian mountains, and a maximum along the U.K. and Ireland western coasts, Northern France and Germany. The same characteristics are also evident in the P99, RX5day, and SDII indices, although for the later the signal is somehow more damped. All these small-scale features are not resolved in the GCM change plots due to the coarser resolution which does not allow the GCMs to adequately resolve orographically forced circulation dynamical and thermodynamical effects and land surface feedback (Chan et al., 2014; Giorgi et al., 2016). The EURO-CORDEX projections have in general a wider spread for both the mid-future and far future time slices followed by CMIP5 and CMIP6, except for the NEU region where the CMIP6 have the highest projection uncertainty.

3.4.2. Drought Frequency Change per Decade and Consecutive Dry Day

The mean annual CDD and the drought frequency change per decade (DF) change are shown in Figure 8 for two time slices and for all ensembles. For both indices a significant maximum is observed over the Mediterranean region with the CDD being positive everywhere and the DF showing the well-known north-south dipole structure (Spinoni et al., 2014), that is, an increase of number of droughts in the south and a decrease in the uppermost northeast European areas and Scandinavia. The CDD spatial structure is quite similar among the three ensembles, with the CMIP6 having longer dry spells for a broader region covering the whole Mediterranean Sea up to the southwestern French coasts and the Alps. An increase in the number of droughts per decade in the Mediterranean is projected by all model ensembles, with a median value of 3 (1.8) for the RCM ensemble, 3.5 (2) for CMIP5 and 4 (2.5) for the CMIP6 ensemble by the far (mid-) century (Figure 9 box plot). The projection uncertainties are quite small (between one and two events per decade) as shown by the CMIP6 and EURO-CORDEX ensembles, respectively. Also, in the NEU region the three ensembles show a consistent (low uncertainty) decrease of the number of droughts between one and two events per decade by the end of century or around one event for the mid-century. The most uncertain region is the CEU, where the zero line is positioned, with a pronounced latitudinal difference between the RCM and CMIP6 ensembles.

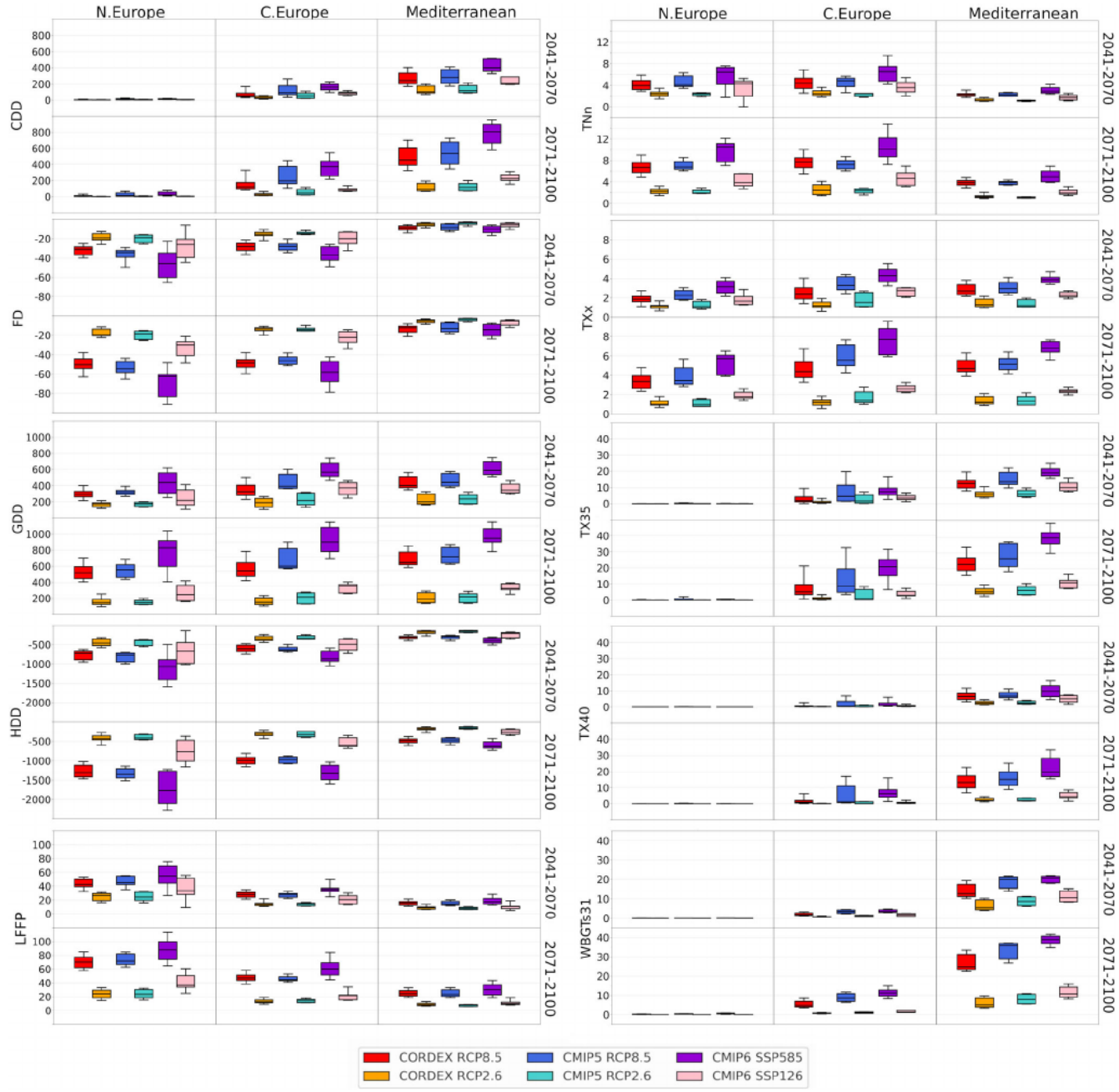

Figure 10. As in Figure 2 for the temperature climate indices: the cooling degree days (CDD, units: degree days), the frost days changes (FD, units = days per year), the growing degree days (TX35, TX40, units = degree days), the heating degree days (HDD, units: degree days), the length of frost-free periods changes (LFFP, units = days), the yearly maximum of daily minimum temperature (TNn, units = °C), the yearly maximum of daily maximum temperature (TXx, units = °C), the number of days per year with maximum temperature over 35°C and 40°C (TX35 and TX40, units = days per year), and the wet bulb globe temperature greater than 31°C (WBGT, units = number of events).

The EURO-CORDEX ensemble has the zero line placed in the southernmost location, going from the United Kingdom through Germany, Austria and the Balkans; the CMIP6 has the line just over southern Sweden and the Baltic Sea, while the CMIP5 zero line lies in between. This uncertainty is reflected in the box plot of Figure 9, where median values spanning from negative to positive are reported when moving from the regional model ensemble to the CMIP6 ensemble (CMIP5 is positioned around the zero-change values) for all the time slices.

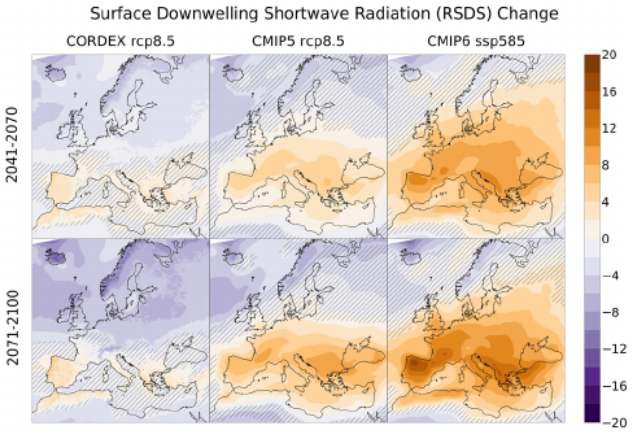

Figure 11. As in Figure 1 for changes in the surface downwelling shortwave radiation (units: W/m^2). Dashed lines cover areas where changes are not significant at the 95% confidence level (Student's t test).

3.5. Simulated Changes for Downward Surface Shortwave Radiation (W/m^2)

Figure 11 shows the periods for the surface downwelling shortwave radiation (rsds) in both scenarios and ensembles.

The common behavior to all ensembles is a tripole pattern, with an increase in rsds over the Mediterranean area and Central Europe and a decrease in Northern Europe and the extreme South of the domain over the Sahara regions. This tripole is likely due to a tripole-like pattern in cloud cover change. Local values reach up to −10 W/m^2 over Northeastern Europe and more than +15 W/m^2 over the Balkans and Southeastern Europe. Note, however, that this tripole pattern is less visible in the CMIP6 ensemble for which the northern pole nearly disappears and the median change over the NEU zone is positive (see Figure 12). For the EURO-CORDEX RCMs and CMIP5 GCMs, the values and spatial patterns obtained in Figures 11 and 12 are in line with previous studies (Bartók et al., 2017, 2019; Boé et al., 2020; Gutiérrez et al., 2019).

An important feature of Figures 11 and 12 is the strong difference between the change signals of the three model ensembles over Central Europe, where the EURO-CORDEX ensemble median values show a decrease in the shortwave radiation reaching the surface for CEU and both periods, whereas both CMIP ensembles show a large increase. This is one of the rare cases of GCM-RCM inconsistency in the climate change response at large scale and confirms the results obtained with CMIP5 and EURO-CORDEX smaller ensembles by Bartók et al. (2017), Boé et al. (2020), Gutiérrez et al. (2019) and Nabat et al. (2020). It has been recently attributed to the different way aerosols are represented currently in GCMs and RCMs (Gutiérrez et al., 2019). In addition, Bartók et al. (2017) showed that cloud cover trends behave very differently in CMIP5 GCMs and EURO-CORDEX RCMs, with a decreasing cloud cover trend in GCMs and an absence of trends in RCMs.

To our knowledge, what differs most between RCMs and GCMs is the temporal evolution of the aerosol forcing (a general decrease of the aerosol load over continental Europe during the scenario period), which is taken into account in CMIP5 and CMIP6 despite large uncertainties, whereas it is not taken into account in most of the EURO-CORDEX RCMs. More specifically, only three RCMs (RACMO22E, ALADIN53 and ALADIN63) apply evolving aerosol forcing in the future, resulting in only 11 runs out of 55 for RCP85 and 5 out of 22 for RCP26.

Looking at individual RCM future responses, for example, for the RCP8.5 and the near-future, we note a strong increase (maximum value of +20 W/m^2) over Central Europe and the Mediterranean for the ALADIN and RACMO22E runs regardless of the versions used and the driving GCM, along with a negative

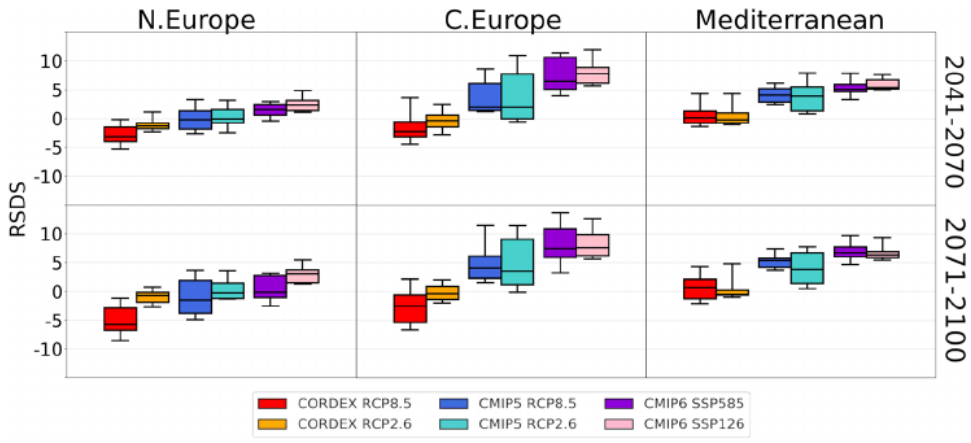

Figure 12. As in Figure 2 for the surface downwelling shortwave radiation (units: W/m^2).

or weakly positive signal for all other RCMs, except for one of the RegCM4–6 runs (not shown). Plotting multimodel mean values for the RCM ensemble in Figure 11 therefore gives a large weight to RCMs without evolving aerosols. Note that the GCM-RCM discrepancy in rsds change also have implications when computing potential photovoltaic production in Europe (Gutiérrez et al., 2019).

It is also worth noting that the change response is largely stronger in CMIP6 than in CMIP5 models. Moreover, the choice of the socio-economic scenario and of the temporal horizon have weak impacts on the results. For example, for the end of the 21st century and the RCP2.6 and SSP126 scenarios, CMIP5 GCMs project an increase by +4 W/m^2 (median value) for the CEU region whereas CMIP6 GCMs project an increase by +7.5 W/m^2 and CORDEX RCMs a decrease by −2 W/m^2. The uncertainty in the future change of surface shortwave radiation is thus dominated by the choice of the model ensemble. Concerning the surface radiation change signal over the European seas, on average the EURO-CORDEX ensemble projects a decrease in surface shortwave radiation over the Baltic and North Seas and a close-to-zero change for the Mediterranean and Black Seas, whatever the scenario and the temporal horizon. Conversely, the CMIP5 ensemble projects nearly no change for the Baltic and North Seas and an increase for the Mediterranean and Black Seas, whereas the CMIP6 ensemble projects a clear and strong increase for all European Seas. These differences in the radiation change signal over the European Seas could have strong impacts on the regional sea physics and marine biogeochemistry scenario simulations, often driven by or coupled to Atmosphere-RCMs (Darmaraki et al., 2019; Gröger et al., 2019; Soto-Navarro et al., 2020). An interesting small-scale feature in the radiation change pattern is the specific signal obtained over the Alps with the CORDEX ensemble for the RCP8.5. Contrary to the GCMs, the RCMs simulate a contrast of response between the Alps (strong decrease in surface shortwave radiation) and the surrounding areas (weak signal or increase). This interesting contrast could be the signature of a potential local added value of the RCMs in future climate response as already shown for summer precipitation by Giorgi et al. (2016). It remains unexplained so far but could be linked to a stronger response of cloud cover over the Alps or to a locally lower influence of the aerosol load decrease.

4. Conclusions

In this paper we investigate and characterize the climate change response over the whole European domain derived from the EURO-CORDEX RCM ensemble, along with CMIP5 and CMIP6 GCM sub-ensembles for two different scenarios (SSP585 or RCP8.5) and (SSP126 or RCP2.6), a far, and a mid-future time slice. The RCM projections are compared with the driving CMIP5 GCM projections and the consistency of the corresponding signals is analyzed. All the results are also put in the context of the new CMIP6 projections, which show a stronger warming signal than CMIP5 due to the higher ECS in several of the models compared to the previous generation GCMs.

For the mean European climate, the well-known south-north seasonal gradients in temperature and precipitation change signals are projected, with maximum warming and increase in precipitation over the northern regions in winter and maximum warming and a significant decrease in precipitation over the southern regions in summer and in particular over the Mediterranean basin. These results confirm previous findings from early regional ensembles such as PRUDENCE and ENSEMBLES, but are able to add a better quantification of the uncertainty and robustness of the signals due to the increased size of the present ensemble.

In both summer and winter, the strongest warming and precipitation responses are always shown by the CMIP6 ensemble. Conversely the EURO-CORDEX ensemble shows the least pronounced warming and precipitation responses. The higher resolution of the RCM ensemble allows for a more detailed description of the warming and precipitation change patterns, showing, for example, higher warming and precipitation responses over mountainous regions, and a much more detailed land-sea contrast along the Mediterranean, Baltic Sea, and Norwegian coasts and islands.

The mean, maximum and minimum temperature projection spread in all seasons and regions is much lower (almost half the magnitude) in the EURO-CORDEX and CMIP5 ensembles than in the CMIP6 one. The mean precipitation change spread is comparable for all the ensembles and is smallest in northern and central Europe in winter and northern Europe in summer.

All the projections agree on an increase of extreme precipitation over the Northern and Central European regions for all selected indices. The results over the Mediterranean region are more contrasted, with some

indices showing no clear trend or even a decrease. For extreme precipitation, the EURO-CORDEX ensemble shows stronger maxima together with fine-scale spatial placement of the signal, for example, minima over the highest elevations and maxima over the Adriatic, Tyrrhenian and Baltic Seas. For extreme precipitation the inter-model agreement is high in terms of the direction of the changes and the inter-model spread is limited to about 10% in northern and central Europe and to less than 15% in the Mediterranean. There is a consensus across models on a small but significant (almost everywhere) increase of dry spell length in north and central Europe and a positive significant change over the Mediterranean basin, confirmed by a unanimous projection of a significant increase in the number of droughts.

The quantification of the uncertainty and robustness of the projections for multiple wet and dry indicators has been presented adding to previous studies like Jacob et al. (2014) and Christensen et al. (2019) that were using a reduced size ensemble with no information on the uncertainty and fewer indices.

For the first time in a comprehensive way we also present an assessment of the impact of climate change on thresholds relevant for one or more socio-economic sectors. These extreme and impact-oriented indices show increasing heat extremes and decreasing cold extremes. In summer, RCMs exhibit a slightly lower signal than their driving CMIP5 GCMs, which themselves exhibit a lower signal than the CMIP6 model ensemble analyzed. For extreme heat indices, the RCMs reveal details not shown by GCMs: low-lying and coastal Mediterranean areas are projected to cross severe heat stress thresholds (e.g., WBGT > 35°C) for up to a few weeks, conditions that are not found in current climate. Indices sensitive to winter temperatures (e.g., length of frost-free period) generally have a larger signal in Northern Europe while indices sensitive to summer temperature (e.g., growing degree day) have a larger signal in Southern Europe.

An overall increase in solar radiation reaching the surface is projected over the Mediterranean region, mostly in response to reduced cloudiness, and a decrease over northern Europe, where cloudiness and precipitation increase. However, the amplitude of these changes as well as the sign of the change over Central Europe remains uncertain and sometimes inconsistent between RCMs and GCMs, specifically in response to varying forcings such as due to aerosols which are treated differently in different models. In general, we find that the future response of surface solar radiation in Europe is very sensitive to the choice of model ensemble and less to the choice of scenario or temporal horizon.

The large EURO-CORDEX high-resolution ensemble, along with the CMIP5 and CMIP6 ones, represent an invaluable resource for climate change studies over the European region. It has been shown how this ensemble provides the basis for application to impact, vulnerability and adaptation studies over the region and for climate service activities. The size of the ensemble, unique for the EURO-CORDEX RCMs, also allows a better characterization of uncertainties in the simulated change signals, an important aspect for end user applications. Here we presented a basic analysis of a set of standard variables and indices necessary to characterize the first-order behavior of the projections in the various ensembles. Our analysis can thus be a first important reference for users of these ensembles.

However, a more in depth and comprehensive analysis of additional features is necessary and is indeed under way, for example, concerning changes in circulation characteristics and regimes, and will be presented in future studies. In addition, an assessment should be conducted on how the present ensemble reproduces observed trends, which would allow an even better characterization of the robustness of the projected change signals. Finally, here we focused on RCM and GCM results, however substantial activities are also under way with the use of empirical-statistical downscaling (ESD) techniques (e.g., Mezghani et al., 2019), which can complement and strengthen the model-based results. All these sources of data will allow an ever better and more in depth assessment of climate change and related impacts over the European region.

Data Availability Statement

All the data used in this work are available on the ESGF. Data are searchable and available for download at the Federated ESGF-CoG Nodes (https://esgf.llnl.gov/nodes.html).

Acknowledgments

The Earth System Grid Federation (ESGF) is an international collaboration with a current focus on serving the World Climate Research Programme's (WCRP) Coupled Model Intercomparison Project (CMIP) and supporting climate and environmental science in general. The work of C. S., M. S., and J. S. is funded by the European Union's Horizon 2020 research and innovation program under Grant Agreement No. 820655 (EXHAUSTION) and the ERANET-SusCROP Cofund Action (RCN Grant No. 299600/E50). IPSL authors thank the CEA TGCC supercomputing center for providing the computer allocation. Part of this study has been funded by the Copernicus Climate Change Service. ECMWF implements this Service on behalf of the European Commission. The RegCM simulations for the ICTP institute have been completed thanks to the support of the CINECA supercomputing center, Bologna, Italy. CLMcom-CCLM-4-8-17 simulations were run on the Piz Daint supercomputer at the Swiss National Supercomputing Centre (CSCS) under project ID s432, and at the German Climate Computing Centre (DKRZ) supported by the German Federal Ministry of Education and Research (BMBF). CLMcom-ETH-COSMO-crCLIM-v1-1 simulations were run on Piz Daint at CSCS under the PRINCIPLES project. ETH acknowledges PRACE for awarding access to Piz Daint at ETH Zürich/CSCS (Switzerland). Four UHOH-WRF361H simulations were funded within the ReKliEs-De project under Grant No. 01LK140 by the BMBF, and one UHOH-WRF361H simulation was funded by the German Science Foundation within the Research Unit 1695. UHOH-WRF361H simulations were run on Hazel Hen at the High Performance Computing Center in Stuttgart (HLRS).

References

Arctic Monitoring and Assessment Programme (AMAP) (2017). Report 'Snow, Water, Ice, Permafrost in the Acrtic'—SWIPA.

Bartók, B., Tobin, I., Vautard, R., Vrac, M., Jin, X., Levavasseur, G., et al. (2019). A climate projection dataset tailored for the European energy sector. *Climate services*, *16*, 100138. https://doi.org/10.1016/j.cliser.2019.100138

Bartók, B., Wild, M., Folini, D., Lüthi, D., Kotlarski, S., Schär, C., et al. (2017). Projected changes in surface solar radiation in CMIP5 global climate models and in EURO-CORDEX regional climate models for Europe. *Climate Dynamics*, *49*(7–8), 2665–2683. https://doi.org/10.1007/s00382-016-3471-2

Boé, J., Somot, S., Corre, L., & Nabat, P. (2020). Large differences in summer climate change over Europe as projected by global and regional climate models: Causes and consequences. *Climate Dynamics*, *54*(5–6), 2981–3002. https://doi.org/10.1007/s00382-020-05153-1

Cannon, A. J., Sobie, S. R., & Murdock, T. Q. (2015). Bias correction of GCM precipitation by quantile mapping: How well do methods preserve changes in quantiles and extremes? *Journal of Climate*, *28*(17), 6938–6959. https://doi.org/10.1175/JCLI-D-14-00754.1

Chan, S. C., Kendon, E. J., Fowler, H. J., Blenkinsop, S., Roberts, N. M., & Ferro, C. A. (2014). The value of high-resolution metoffice regional climate models in the simulation of multihourly precipitation extremes. *Journal of Climate*, *27*(16), 6155–6174. https://doi.org/10.1175/JCLI-D-13-00723.1

Christensen, J. H., & Christensen, O. B. (2007). A summary of the PRUDENCE model projection of changes in European climate by the end of this century. *Climate Change*, *81*, 1–6. https://doi.org/10.1007/s10584-006-9211-6

Christensen, J. H., Larsen, M. A., Christensen, O. B., Drews, M., & Stendel, M. (2019). Robustness of European climate projections from dynamical downscaling. *Climate Dynamics*, *53*(7–8), 4857–4869. https://doi.org/10.1007/s00382-019-04831-z

Dai, A., Luo, D., Song, M., & Liu, J. (2019). Arctic amplification is caused by sea-ice loss under increasing CO_2. *Nature Communications*, *10*(1), 121. https://doi.org/10.1038/s41467-018-07954-9

Darmaraki, S., Somot, S., Sevault, F., Nabat, P., Cabos, W., Cavicchia, L., et al. (2019). Future evolution of marine heat waves in the Mediterranean Sea. *Climate Dynamics*, *53*(3–4), 1371–1392. https://doi.org/10.1007/s00382-019-04661-z

Déqué, M., Rowell, D. P., Lüthi, D., Giorgi, F., Christensen, J. H., Rockel, B., et al. (2007). An intercomparison of regional climate simulations for Europe: Assessing uncertainties in model projections. *Climatic Change*, *81*(S1), 53–70. https://doi.org/10.1007/s10584-006-9228-x

Déqué, M., Somot, S., Sanchez-Gomez, E., Goodess, C. M., Jacob, D., Lenderink, G., & Christensen, O. B. (2012). The spread amongst ENSEMBLES regional scenarios: Regional climate models, driving general circulation models and interannual variability. *Climate Dynamics*, *38*(5–6), 951–964. https://doi.org/10.1007/s00382-011-1053-x

Deser, C., Phillips, A., Bourdette, V., & Teng, H. (2012). Uncertainty in climate change projections: The role of internal variability. *Climate Dynamics*, *38*(3–4), 527–546. https://doi.org/10.1007/s00382-010-0977-x

Evin, G., Hingray, B., Blanchet, J., Eckert, N., Morin, S., & Verfaillie, D. (2019). Partitioning uncertainty components of an incomplete ensemble of climate projections using data augmentation. *Journal of Climate*, *32*(8), 2423–2440. https://doi.org/10.1175/JCLI-D-18-0606.1

Eyring, V., Bony, S., Meehl, G. A., Senior, C. A., Stevens, B., Stouffer, R. J., & Taylor, K. E. (2016). Overview of the Coupled Model Intercomparison Project Phase 6 (CMIP6) experimental design and organization. *Geoscientific Model Development (Online)*, *9*(5), 1937–1958. https://doi.org/10.5194/gmd-9-1937-2016

Forster, P. M., Maycock, A. C., McKenna, C. M., & Smith, C. J. (2020). Latest climate models confirm need for urgent mitigation. *Nature Climate Change*, *10*(1), 7–10. https://doi.org/10.1038/s41558-019-0660-0

Giorgi, F. (2006). Climate change hot-spots. *Geophysical Research Letters*, *33*, L08707. https://doi.org/10.1029/2006GL025734

Giorgi, F., & Coppola, E. (2007). The European Climate-Change Oscillation (ECO). *Geophysical Research Letters*, *34*, L217003. https://doi.org/10.1029/2007GL031223

Giorgi, F., & Coppola, E. (2010). Does the model regional bias affect the projected regional climate change? An analysis of global model projections. *Climatic Change*, *100*(3–4), 787–795. https://doi.org/10.1007/s10584-010-9864-z

Giorgi, F., Coppola, E., & Raffaele, F. (2018). Threatening levels of cumulative stress due to hydroclimatic extremes in the 21st century. *Climate and Atmospheric Science*, *1*(1), 1–9.

Giorgi, F., & Lionello, P. (2008). Climate change projections for the Mediterranean region. *Global and Planetary Change*, *63*(2–3), 90–104. https://doi.org/10.1016/j.gloplacha.2007.09.005

Giorgi, F., Torma, C., Coppola, E., Ban, N., Schär, C., & Somot, S. (2016). Enhanced summer convective rainfall at Alpine high elevations in response to climate warming. *Nature Geoscience*, *9*(8), 584–589. https://doi.org/10.1038/ngeo2761

Gröger, M., Arneborg, L., Dieterich, C., Höglund, A., & Meier, H. E. M. (2019). Summer hydrographic changes in the Baltic Sea, Kattegat and Skagerrak projected in an ensemble of climate scenarios downscaled with a coupled regional ocean–sea ice–atmosphere model. *Climate Dynamics*, *53*(9–10), 5945–5966. https://doi.org/10.1007/s00382-019-04908-9

Gutiérrez, C., Somot, S., Nabat, P., Mallet, M., Corre, L., van Meijgaard, E., et al. (2019). Future evolution of surface solar radiation and photovoltaic potential in Europe: Investigating the role of aerosols. *Environmental Research Letters*, *15*(3), 034035.

Hawkins, E., & Sutton, R. (2009). The potential to narrow uncertainty in regional climate predictions. *Bulletin of the American Meteorological Society*, *90*(8), 1095–1108. https://doi.org/10.1175/2009BAMS2607.1

Hewitt, C. D., & Griggs, D. J. (2004). Ensembles-based predictions of climate changes and their impacts. *Eos*, *85*(52), 566. https://doi.org/10.1029/2004EO520005

Hodnebrog, Ø., Myhre, G., Samset, B. H., Alterskjær, K., Andrews, T., Boucher, O., & Kirkevåg, A. (2019). Water vapour adjustments and responses differ between climate drivers. *Atmospheric Chemistry and Physics*, *19*(20), 12,887–12,899.

Iturbide, M., Gutiérrez, J. M., Alves, L. M., Bedia, J., Cerezo-Mota, R., Cimadevilla, E., et al. (2020). An update of IPCC climate reference regions for subcontinental analysis of climate model data: Definition and aggregated datasets. *Earth System Science Data*, *12*(4), 2959–2970.

Jacob, D., Petersen, J., Eggert, B., Alias, A., Christensen, O. B., Bouwer, L. M., et al. (2014). EURO-CORDEX: New high-resolution climate change projections for European impact research. *Regional Environmental Change*, *14*(2), 563–578. https://doi.org/10.1007/s10113-013-0499-2

Jacob, D., Teichmann, C., Sobolowski, S., Katragkou, E., Anders, I., Belda, M., et al. (2020). Regional climate downscaling over Europe: Perspectives from the EURO-CORDEX community. *Regional Environmental Change*, *53*(1–2), 759–778. https://doi.org/10.1007/s00382-019-04612-8

Kjellström, E., Nikulin, G., Strandberg, G., Christensen, O. B., Jacob, D., Keuler, K., et al. (2018). European climate change at global mean temperature increases of 1.5 and 2°C above pre-industrial conditions as simulated by the EURO-CORDEX regional climate models. *Earth System Dynamics*, *9*, 459–478, 2018, https://doi.org/10.5194/esd-9-459-2018, https://www.earth-syst-dynam-discuss.net/esd-2017-104/. Special Issue: The Earth system at a global warming of 1.5°C and 2.0°C

Kjellström, E., Thejll, P., Rummukainen, M., Christensen, J. H., Boberg, F., Christensen, O. B., & Fox Maule, C. (2013). Emerging regional climate change signals for Europe under varying large-scale circulation conditions. *Climate Research*, *56*(2), 103–119. https://doi.org/10.3354/cr01146

Kotlarski, S., Keuler, K., Christensen, O. B., Colette, A., Déqué, M., Gobiet, A., & Nikulin, G. (2014). Regional climate modeling on European scales: A joint standard evaluation of the EURO-CORDEX RCM ensemble. *Geoscientific Model Development*, *7*(4), 1297–1333. https://doi.org/10.5194/gmd-7-1297-2014

McCabe, G. J., Betancourt, J. L., & Feng, S. (2015). Variability in the start, end, and length of frost-free periods across the conterminous United States during the past century. *International Journal of Climatology*, *35*(15), 4673–4680. https://doi.org/10.1002/joc.4315

Mezghani, A., Dobler, A., Benestad, R., Haugen, J. E., Parding, K. M., Piniewski, M., & Kundzewicz, Z. W. (2019). Subsampling impact on the climate change signal over Poland based on simulations from statistical and dynamical downscaling. *Journal of Applied Meteorology and Climatology*, *58*(5), 1061–1078. https://doi.org/10.1175/JAMC-D-18-0179.1

Mora, C., Spirandelli, D., Franklin, E. C., Lynham, J., Kantar, M. B., Miles, W., et al. (2018). Broad threat to humanity from cumulative climate hazards intensified by greenhouse gas emissions. *Nature Climate Change*, *8*(12), 1062–1071. https://doi.org/10.1038/s41558-018-0315-6

Moss, R. H., Edmonds, J. A., Hibbard, K. A., Manning, M. R., Rose, S. K., Van Vuuren, D. P., & Meehl, G. A. (2010). The next generation of scenarios for climate change research and assessment. *Nature*, *463*(7282), 747–756. https://doi.org/10.1038/nature08823

Nabat, P., Somot, S., Cassou, C., Mallet, M., Michou, M., Bouniol, D., et al. (2020). Modulation of radiative aerosols effects by atmospheric circulation over the Euro-Mediterranean region. *Atmospheric Chemistry and Physics Discussions*, in review, *20*, 8315–8349. https://doi.org/10.5194/acp-20-8315-2020

Nabat, P., Somot, S., Mallet, M., Sanchez-Lorenzo, A., & Wild, M. (2014). Contribution of anthropogenic sulfate aerosols to the changing Euro-Mediterranean climate since 1980. *Geophysical Research Letters*, *41*, 5605–5611. https://doi.org/10.1002/2014GL060798

Rajczak, J., & Schär, C. (2017). Projections of future precipitation extremes over Europe: A multimodel assessment of climate simulations. *Journal of Geophysical Research: Atmospheres*, *122*, 10–773.

Riahi, K., van Vuuren, D. P., Kriegler, E., Edmonds, J., O'Neill, B. C., Fujimori, S., et al. (2017). The shared socioeconomic pathways and their energy, land use, and greenhouse gas emissions implications: An overview. *Global Environmental Change*, *42*, 153–168. https://doi.org/10.1016/j.gloenvcha.2016.05.009

Ruosteenoja, K., Markkanen, T., Venäläinen, A., Räisänen, P., & Peltola, H. (2018). Seasonal soil moisture and drought occurrence in Europe in CMIP5 projections for the 21st century. *Climate Dynamics*, *50*(3–4), 1177–1192. https://doi.org/10.1007/s00382-017-3671-4

Ruosteenoja, K., Räisänen, J., Venäläinen, A., & Kämäräinen, M. (2016). Projections for the duration and degree days of the thermal growing season in Europe derived from CMIP5 model output. *International Journal of Climatology*, *36*(8), 3039–3055. https://doi.org/10.1002/joc.4535

Russo, S., Sillmann, J., & Fischer, E. (2015). Top ten European heatwaves since 1950 and their occurrence in the coming decades. *Environmental Research Letters*, *10*(12), 124003. https://doi.org/10.1088/1748-9326/10/12/124003

Ruti, P. M., Somot, S., Giorgi, F., Dubois, C., Flaounas, E., Obermann, A., et al. (2016). MED-CORDEX initiative for Mediterranean climate studies. *Bulletin of the American Meteorological Society*, *97*(7), 1187–1208. https://doi.org/10.1175/BAMS-D-14-00176.1

Schwingshackl, C., Davin, E. L., Hirschi, M., Sørland, S. L., Wartenburger, R., & Seneviratne, S. I. (2019). Regional climate model projections underestimate future warming due to missing plant physiological CO_2 response. *Environmental Research Letters*, *14*, 114019. https://doi.org/10.1088/1748-9326/ab4949

Somot, S., Ruti, P., Ahrens, B., Coppola, E., Jordà, G., Sannino, G., & Solmon, F. (2018). Editorial for the Med-CORDEX special issue. *Climate Dynamics*, *51*(3), 771–777. https://doi.org/10.1007/s00382-018-4325-x

Sørland, S. L., Schär, C., Lüthi, D., & Kjellström, E. (2018). Bias patterns and climate change signals in GCM-RCM model chains. *Environmental Research Letters*, *13*(7), 074017. https://doi.org/10.1088/1748-9326/aacc77

Soto-Navarro, J., Jordá, G., Amores, A., Cabos, W., Somot, S., Sevault, F., et al. (2020). Evolution of Mediterranean Sea water properties under climate change scenarios in the Med-CORDEX ensemble. *Climate Dynamics*, *54*(3-4), 2135–2165. https://doi.org/10.1007/s00382-019-05105-4

Spinoni, J., Barbosa, P., Bucchignani, E., Cassano, J., Cavazos, T., Christensen, J. H., et al. (2020). Future global meteorological drought hotspots: A study based on CORDEX data. *Journal of Climate*, *33*(9), 3635–3661. https://doi.org/10.1175/JCLI-D-19-0084.1

Spinoni, J., Naumann, G., Carrao, H., Barbosa, P., & Vogt, J. (2014). World drought frequency, duration, and severity for 1951–2010. *International Journal of Climatology*, *34*, 2792–2804. https://doi.org/10.1002/joc.3875

Spinoni, J., Vogt, J., & Barbosa, P. (2015). European degree-day climatologies and trends for the period 1951–2011. *International Journal of Climatology*, *35*(1), 25–36. https://doi.org/10.1002/joc.3959

Taylor, K. E., Stouffer, R. J., & Meehl, G. A. (2012). An overview of CMIP5 and the experiment design. *Bulletin of the American Meteorological Society*, *93*(4), 485–498. https://doi.org/10.1175/BAMS-D-11-00094.1

Tramblay, Y., & Somot, S. (2018). Future evolution of extreme precipitation in the Mediterranean. *Climatic Change*, *151*(2), 289–302. https://doi.org/10.1007/s10584-018-2300-5

Van der Linden, P., & Mitchell, J. F. (Eds.). (2009). ENSEMBLES: Climate change and its impacts: Summary of research and results from ENSEMBLES project. *Met Office Hadley Centre, Exeter*.

Vautard, R., Gobiet, A., Sobolowski, S., Kjellström, E., Stegehuis, A., Watkiss, P., et al. (2014). The European climate under a 2°C global warming. *Environmental Research Letters*, *9*(3), 034006. https://doi.org/10.1088/1748-9326/9/3/034006

Vautard, R., Kadygrov, N., Iles, C., Boberg, F., Buonomo, E., Bülow, K., et al. (2020). Evaluation of the large EURO-CORDEX regional climate model ensemble. *Journal of Geophysical Research: Atmospheres*, *125*, e2019JD032344. https://doi.org/10.1029/2019JD032344

Walsh, J. E. (2014). Intensified warming of the Arctic: Causes and impacts on mid-latitudes. *Global and Planetary Change*, *117*, 52–63. https://doi.org/10.1016/j.gloplacha.2014.03.003

Zelinka, M. D., Myers, T. A., McCoy, D. T., Po-Chedley, S., Caldwell, P. M., Ceppi, P., et al. (2020). Causes of higher climate sensitivity in CMIP6 models. *Geophysical Research Letters*, *47*, e2019GL085782. https://doi.org/10.1029/2019GL085782